Geochemistry Geophysics Geosystems G3

Article
Volume 12
12 May 2011
Q0AB07, doi:10.1029/2010GC003316
ISSN: 1525-2027

Published by AGU and the Geochemical Society

Thin oceanic crust and flood basalts: India-Seychelles breakup

J. J. Armitage
Department of Earth Science and Engineering, Imperial College London, South Kensington Campus, London SW7 2AZ, UK

Now at the Institut de Physique du Globe de Paris, 1 rue Jussieu, F-75238 Paris CEDEX 05, France (armitage@ipgp.fr)

J. S. Collier
Department of Earth Science and Engineering, Imperial College London, South Kensington Campus, London SW7 2AZ, UK (jenny.collier@imperial.ac.uk)

T. A. Minshull and T. J. Henstock
National Oceanography Centre, Southampton, University of Southampton, European Way, Southampton SO14 3ZH, UK (tmin@noc.soton.ac.uk; then@noc.soton.ac.uk)

[1] Recent seismic experiments showed that separation of India from the Seychelles occurred in two phases of rifting. The first brief phase of rifting between India and the Laxmi Ridge formed the Gop Rift, which is characterized by thick oceanic crust and underplating of the adjacent continental margins. The age of the Gop Rift is uncertain, initiation of seafloor spreading being some time between 71 and 66 Ma. This was then followed by rifting and seafloor spreading between the Laxmi Ridge and the Seychelles, the onset of which is well dated by magnetic anomalies at 63.4 Ma and characterized by thin oceanic crust. Both of these rift events occurred within 1000 km of the center of the Deccan flood basalts, which formed at 65 ± 1 Ma. To constrain the age of the Gop Rift and to explore the reasons for the change in crustal structure between the Gop Rift and Seychelles-Laxmi Ridge margins, we employ a geodynamic model of rift evolution in which melt volumes, seismic velocity, and rare earth element (REE) chemistry of the melt are estimated. We explore the consequences of different thermal structures, hydration, and depletion on the melt production during the India-Seychelles breakup to understand the reasons behind the thin oceanic crust observed. Magmatism at the Gop Rift is consistent with a model in which the seafloor spreading began at 71 Ma, ca. 6 Myr prior to the Deccan. The opening occurred above a hot mantle layer (temperature of 200°C, thickness of 50 km) that we interpret as incubated Deccan material, which had spread laterally beneath the lithosphere. This scenario is consistent with observed lower crustal seismic velocities of 7.4 km s^{-1} and 12 km igneous crustal thickness. The model indicates that when the seafloor spreading migrated to the Seychelles-Laxmi Ridge at 63 Ma, the thermal anomaly was reduced significantly but not sufficient to explain the observed reduction in breakup magmatism. From observations here of 5.2 km oceanic crust, lower crustal seismic velocities of 6.9 km s^{-1} and a flat REE profile, we infer that breakup occurred in a region of mantle that became depleted by prior extension related to the Gop Rift.

Components: 14,800 words, 14 figures, 4 tables.

Keywords: Indian continental margin; rifting; volcanic passive margin; nonvolcanic passive margin; melt generation.

Index Terms: 8137 Tectonophysics: Hotspots, large igneous provinces, and flood basalt volcanism; 8105 Tectonophysics: Continental margins: divergent (1212, 8124); 8120 Tectonophysics: Dynamics of lithosphere and mantle: general (1213).

Received 4 August 2010; **Revised** 22 February 2011; **Accepted** 7 March 2011; **Published** 12 May 2011.

Armitage, J. J., J. S. Collier, T. A. Minshull, and T. J. Henstock (2011), Thin oceanic crust and flood basalts: India-Seychelles breakup, *Geochem. Geophys. Geosyst.*, *12*, Q0AB07, doi:10.1029/2010GC003316.

Theme: Magma-Rich Extensional Regimes
Guest Editors: R. Meyer, J. van Wijk, A. Breivik, and C. Tegner

1. Introduction

[2] The northwest Indian Ocean opened in two phases of rifting between the Indian continent and the continental block that forms the Seychelles plateau [*Bhattacharya et al.*, 1994; *Minshull et al.*, 2008]. The first phase of rifting and brief seafloor spreading formed the Gop Rift and Laxmi Basin. This was then followed by rifting and seafloor spreading between the Laxmi Ridge and the Seychelles, which continues today at the Carlsberg Ridge (Figure 1). The Laxmi Ridge is therefore interpreted as a fragment of continental lithosphere that also became detached from the Indian continent, and has been mapped beneath the thick sediments of this part of the Indian Ocean by a distinctive negative free-air gravity anomaly [*Naini and Talwani*, 1982]. Magnetic data show that the two rifting events occurred around the time of the formation of the Deccan flood basalts, which was between 69 and 63 Ma [*Pande*, 2002; *Courtillot and Renne*, 2003]. Therefore, it could be expected that both the Gop Rift and Seychelles-Laxmi margins would show signs of excess magmatism, as is observed in the North Atlantic where the rifted margin formed around the time of the flood basalt volcanism in Greenland and northwest Europe [e.g., *White and McKenzie*, 1989]. Here we report a detailed study of the formation of the Northwest Indian Ocean, focusing on understanding the timing of events that led to the breakup of the Seychelles microcontinent from India.

[3] During the opening of the Gop Rift up to 12 km of igneous material was emplaced beneath the Indian subcontinent, Laxmi Ridge and Seychelles plateau and 9 km thick oceanic crust was formed (Figure 2). Unfortunately the Gop Rift is just 100 km wide, making it impossible to date uniquely from seafloor spreading anomalies. Recent forward modeling of currently available magnetic data has suggested that either it predates or is synchronous with the Deccan flood basalts at 65 Ma [*Minshull et al.*, 2008; *Collier et al.*, 2008; *Yatheesh et al.*, 2009]. Note that in the magnetic models of *Yatheesh et al.* [2009] a basement high known as the Palitana Ridge is assumed to be the extinct spreading axis in the center of the Gop Rift, whereas in the models of *Minshull et al.* [2008] and *Collier et al.* [2008] the axis lies on the southern boundary of the Gop Rift, near the junction with the continental crust of the Laxmi Ridge. The latter interpretation is consistent with that of *Malod et al.* [1997], who first recognized the Palitana Ridge, and is based on an identification of the region of oceanic crust from wide-angle seismic data [*Minshull et al.*, 2008; *Collier et al.*, 2008]. As a result of their differing interpretation of the extent of oceanic crust of the Gop Rift, the models of *Malod et al.* [1997], *Minshull et al.* [2008] and *Collier et al.* [2008] show the Palitana Ridge to have a central positive magnetic anomaly (and hence to have formed during a reversed polarity chron), whereas the interpretation of *Yatheesh et al.* [2009, Figure 8] show a central negative anomaly (normal polarity chron). For this reason we do not draw on the models of *Yatheesh et al.* [2009] further. *Minshull et al.* [2008] and *Collier et al.* [2008] propose several different scenarios for the age and spreading rate of the oceanic crust within the Gop Rift. The first aim of the modeling work presented here is to test the ability of these previously proposed scenarios to match the observed magmatism determined from seismic observations and so to provide an independent constraint on the age of the Gop Rift.

[4] The oldest oceanic crust between the Laxmi Ridge and Seychelles is of anomaly 28n age (63.4 Ma [*Collier et al.*, 2008]). Yet here the oceanic crust is anomalously thin (5.2 km [*Collier et al.*, 2009]). The presence of thin oceanic crust so close to regions of magmatic intrusions (underplate) is hard to reconcile using conventional ideas of volcanic and nonvolcanic margin formation. Recently we presented the model of the Seychelles-India breakup that best fit the possible ages of the formation of the Gop Rift [*Armitage et al.*, 2010]. We showed that the formation of the Gop Rift consequently thinned and depleted the upper mantle prior to breakup. The second aim of the modeling work presented here is to more fully examine the

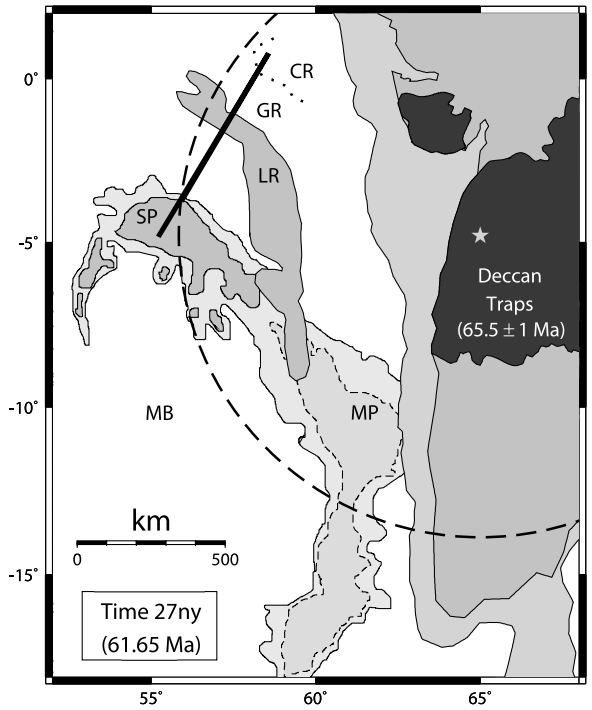

Figure 1. The northwest Indian Ocean, reconstructed using the 27ny (61.65 Ma [*Gradstein et al.*, 2005]) Euler rotation pole of *Royer et al.* [2002] (Lat 18.83°, Lon 24.86°, Angle 35.411°). SP, Seychelles Plateau; LR, Laxmi Ridge; GR, Gop Rift; CR, Continental Rise; MP, Mascarene Plateau; MB, Mascarene Basin. The black line indicates the reconstructed profile of Figure 2, and the dashed line shows the 1000 km radius from the Deccan Traps. The oldest seafloor spreading anomaly in the northern Mascarene Basin is 33n [*Bernard and Munschy*, 2000], and north of the Seychelles Plateau is 28n [*Collier et al.*, 2008].

parameter space and highlight the uncertainties when exploring multiple phase rifting.

2. Methods

2.1. Geodynamics

2.1.1. Equations of Mantle Creep

[5] We wish to investigate the control mantle temperature, composition (depletion) and half-spreading rates have on the evolution of the northwest Indian Ocean. We have employed the 2-D viscous model of the upper mantle, the asthenosphere and lithosphere, down to 700 km depth [*Armitage et al.*, 2009], which was developed from Citcom [*Nielsen and Hopper*, 2004; *Moresi and Solomatov*, 1995], to the extension and breakup of the Seychelles from India. Stokes equations of flow are solved assuming that density variations are sufficiently small that they only affect gravitational forces, the Bousinesq approximation. We also assume that within the conservation of mass we can neglect the effect of density changes from mass transfer due to melting [*Cordery and Phipps Morgan*, 1993]. Therefore, Stokes equations are written, in tensor notation, as follows: conservation of mass,

$$\frac{\partial u_i}{\partial x_i} = 0, \tag{1}$$

the conservation of momentum for an incompressible fluid which undergoes melting when crossing the solidus,

$$\frac{\partial \tau_{ij}}{\partial x_j} + \frac{\partial p}{\partial x_i} = \Delta\rho\lambda_i, \tag{2}$$

and finally the conservation of energy [from *Scott*, 1992],

$$\frac{\partial T}{\partial t} = -u_i\frac{\partial T}{\partial x_i} + \kappa\frac{\partial^2 T}{\partial x_j^2} - \frac{L\dot{m}}{c_p} \tag{3}$$

We use the standard summation convention where repeated indices are summed. The u is the solid mantle creep, T is the mantle temperature, τ is the deviatoric stress tensor, $\Delta\rho$ is the density change due to temperature and the generation of melt [see *Nielsen and Hopper*, 2004], $\dot{m}$ is the melt production rate, κ is the thermal diffusivity, L is the latent heat of melting and λ_i is a unit vector in the vertical direction (i.e., $\lambda_1 = 0$, $\lambda_2 = 1$). A list of parameters used can be found in Table 1. The latent heat of melting is given by

$$L = T_m\Delta S, \tag{4}$$

where T_m is a mantle reference temperature of 1598 K and ΔS is the change in entropy upon melting. We model the mantle assuming a non-Newtonian rheology as defined in the study by *Nielsen and Hopper* [2004]. The details of these equations and how they are solved are covered by *Armitage et al.* [2008] and *Nielsen and Hopper* [2004].

2.1.2. Decompression Melting of the Mantle

[6] The primary melts that generate typical mid-ocean ridge basalts (MORB) with 10%–13% MgO are estimated to be formed at mantle potential temperatures in the range of 1280 to 1400°C [*Herzberg et al.*, 2007]. Previous models of rifting have used various mantle temperatures that generally fall within this range. The choice of potential temperature, however, is quite important. *McKenzie et al.* [2005] show that at mid-ocean ridges a 12.5°C

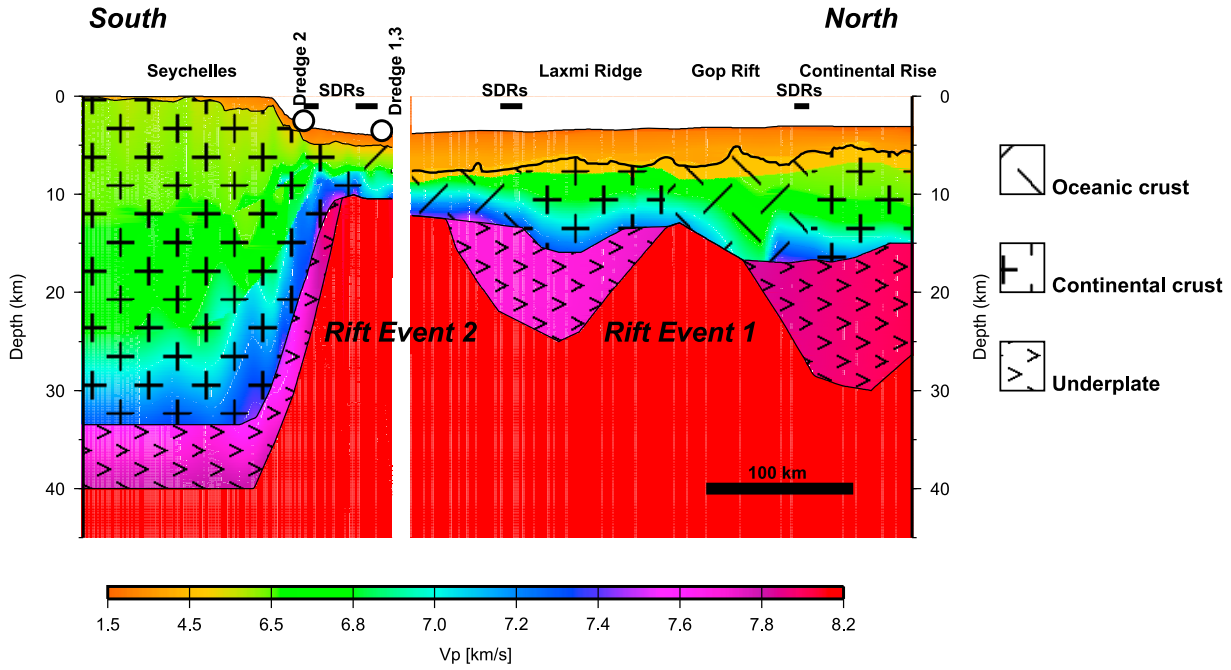

Figure 2. Seismic structure of the conjugate Seychelles-Laxmi Ridge margins (see Figure 1 for line location). The data for each margin were modeled independently; the methods are described by *Collier et al.* [2009] and *Minshull et al.* [2008]. SDRS, seaward dipping reflectors.

increase in mantle temperature increases crustal thickness by 1 km. Therefore, we explore a range of background mantle temperatures. Melt generation is also dependent on the change in entropy (ΔS). Thermodynamic and experimental work suggest that ΔS is around 300 to 400 J K^{-1} kg^{-1} at depths up to 3 GPa [*Kojitani and Akaogi*, 1997; *Hirschmann et al.*, 1999]. Following the experimental work of *Kojitani and Akaogi* [1997] we use the upper bound calculated by *Hirschmann et al.* [1999] of a change in entropy of 400 J K^{-1} kg^{-1}.

[7] In this study, as well as the effect of mantle potential temperature and spreading rates on the rifted margin formation, we will investigate the effect of mantle depletion and dehydration. Therefore, we review the basic equations and assumptions that allow us to simulate these effects. Following *Scott* [1992], the advection of the residue due to melting, X, which is the concentration of a perfectly compatible trace element, is given by

$$\frac{\partial X}{\partial t} = -u_i \frac{\partial X}{\partial x_i} + \frac{X}{1-\phi}\dot{m}, \tag{5}$$

where ϕ is melt porosity, $\dot{m}$ is the melt production rate (Table 1; for further derivation see Appendix A). This concentration, X, of a perfectly compatible trace element is always positive, and equal to one when no melting has occurred. Values of X greater than one indicate material from which melt has been extracted, values less than one indicate material which has had melt added by in situ freezing [*Scott*, 1992]. Assuming batch melting, where the melt remains in equilibrium within the melting column and is only removed at the upper boundary [*Plank et al.*, 1995], the quantity X can be related to a degree of depletion due to melting F, as defined in the study by *Scott* [1992], by

$$X(1-F) = 1. \tag{6}$$

Therefore, for small melt fractions $\Delta X \approx \Delta F$.

[8] The melt production rate, $\dot{m}$, couples the energy balance (equation (3)) and equation of continuity of composition (equation (5)). To calculate $\dot{m}$, a solidus is defined. Normally the solidus is defined as a function of depth. However here following *Scott* [1992] and *Phipps Morgan* [2001] it is a function of depth and depletion X,

$$T_s^{real} = T_{s0} + z\left(\frac{\partial T_s}{\partial z}\right)_X + \left(\frac{\partial T_s}{\partial X}\right)_z (X-1), \tag{7}$$

where T_{S0} is the dry solidus temperature at the surface ($z = 0$). T_s^{real} is converted to a potential temperature by correcting for the adiabatic temperature change,

$$\left(\frac{\partial T}{\partial z}\right)_S = \frac{g\alpha T}{c_p}, \tag{8}$$

Table 1. Model Parameters and Assumed Values

Variable	Meaning and Units	Value
c_p	specific heat capacity, J kg^{-1} K^{-1}	1200
C	instantaneous major element melt composition	
$\overline{C}$	mean major element melt composition	
g	acceleration of gravity, m s^{-2}	9.8
F	melt depletion	
h_c	crustal thickness, km	
L	latent heat upon melting, J mol^{-1}	
$\dot{m}$	dimensionless melt production rate	
p	pressure, Pa	
ΔS	change in entropy upon melting	400 J K^{-1} kg^{-1}
T	mantle temperature, K	
T_m	mantle reference temperature	1598 K
T_s	wet or dry solidus temperature, K	
T_{s0}	dry solidus surface temperature, K	1373
u	mantle creep, m s^{-1}	
V_p	lower crustal seismic velocity, km s^{-1}	
X	concentration of perfectly compatible trace element	
α	coefficient of thermal expansion	3.3 × 10^{-5} K^{-1}
$\dot{\epsilon}$	strain rate, s^{-1}	
κ	thermal diffusivity, m^2 s^{-1}	10^{-6}
η	viscosity, Pa s	
ϕ	retained melt (porosity)	
ρ_m	mantle reference density, Kg m^{-3}	3340
ρ_l	melt density, Kg m^{-3}	2800
$\Delta\rho$	density change due to temperature and melt generation	
τ	deviatoric stress, Pa	

leading to the solidus for a dry mantle rock,

$$T_s^{dry} = T_{s0} + z\left(\left(\frac{\partial T_s}{\partial z}\right)_X - \left(\frac{\partial T}{\partial z}\right)_S\right) + \left(\frac{\partial T_s}{\partial X}\right)_z (X-1). \quad (9)$$

The dependence on depletion adjusts the solidus as melting continues. The depth derivative of the solidus at constant depletion $(\partial T_s/\partial z)_X$ is assumed to be 3.4 × 10^{-3} K m^{-1} [*Scott*, 1992]. The depletion derivative of the solidus at constant depth $(\partial T_s/\partial x)_z$, or solidus depletion gradient, changes depending on the prior depletion of the lithosphere. The solidus depletion gradient is relatively poorly constrained. For mantle olivine compositions, the gradient has been previously estimated at between 200 and 440°C [*Scott*, 1992; *Phipps Morgan*, 2001]. As melting progresses the gradient increases. Recent experiments on synthetic depleted mantle peridotite show that the solidus depletion gradient is ~300°C for the melting of a spinel lherzolite residual assemblage, a fertile mantle source [*Wasylenki et al.*, 2003]. The gradient increases to ~900°C for a harzburgite residual assemblage, a more depleted mantle source [*Wasylenki et al.*, 2003]. An increase in the solidus depletion gradient from the melting of an increasingly depleted source is also predicted from thermodynamic calculations [*Hirschmann et al.*, 1999]. To explore the effect of this change in solidus depletion gradient within a rift setting we varied this gradient from 300 to 800°C to simulate the melting of an increasingly depleted source mantle rock.

2.1.3. Decompression Melting of a Wet Mantle

[9] Melting of a mantle that contains volatiles such as water is now generally accepted to increase the depth of melting by ~50 km and increase the mantle viscosity by two orders of magnitude [*Hirth and Kohlstedt*, 1996; *Mei and Kohlstedt*, 2000; *Dixon et al.*, 2002; *Asimow and Langmuir*, 2003; *Hirschmann*, 2006]. Following *Armitage et al.* [2008], we introduce a wet solidus. The definition of this solidus follows *Braun et al.* [2000] and *Nielsen and Hopper* [2004], and is up to ΔT_s = 200°C cooler than the dry solidus. The wet solidus is given by

$$T_s^{wet} = T_s^{dry} - \Delta T_s \frac{1.02 - X}{\Delta X}, \quad (10)$$

where wet melting occurs until a melt fraction of 2%, ΔX = 0.02, is generated, or depletion X = 1.02 (Figure 3). Beyond this point the mantle is assumed to be dry and the dry solidus defined in equation (9) is used.

[10] Wet mantle melts at greater pressures but melt production is low until the mantle dries out at about 2% melt depletion [*Braun et al.*, 2000], therefore

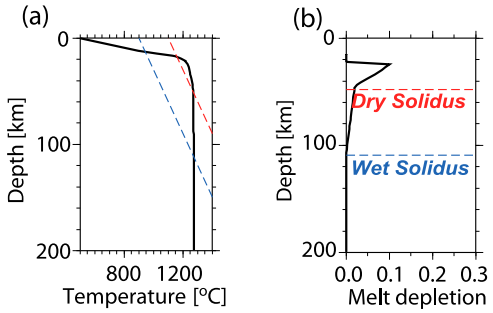

Figure 3. Typical temperature and melt fraction generated at the center of extension for extension of 125 km thick lithosphere with no thermal anomaly (see Figure 4). (a) A typical geotherm, showing the wet and the dry solidus. (b) Melt depletion against depth, showing again the dry and wet solidus and the increased melt productivity during melting of a dry mantle.

the melt production rate is altered correspondingly (Figure 3). The melt production rate is calculated at each time step by calculating the position of the wet or dry solidus. The methods for these calculations are outlined by *Armitage et al.* [2009]. The igneous crustal thickness, h_c, can then be calculated, as defined by *Ito et al.* [1996],

$$h_c = \frac{2}{u_z}\left(\frac{\rho_m}{\rho_l}\right)\int\int_{melt} \dot{m}dxdz, \qquad (11)$$

where the averages are over the melt region and u_z is the vertical velocity at the ridge axis, ρ_m is a mantle reference density and ρ_l is the melt density.

2.2. Model Initial Conditions

[11] Models are for a region of the lithosphere and asthenosphere 700 km deep by 2800 km wide

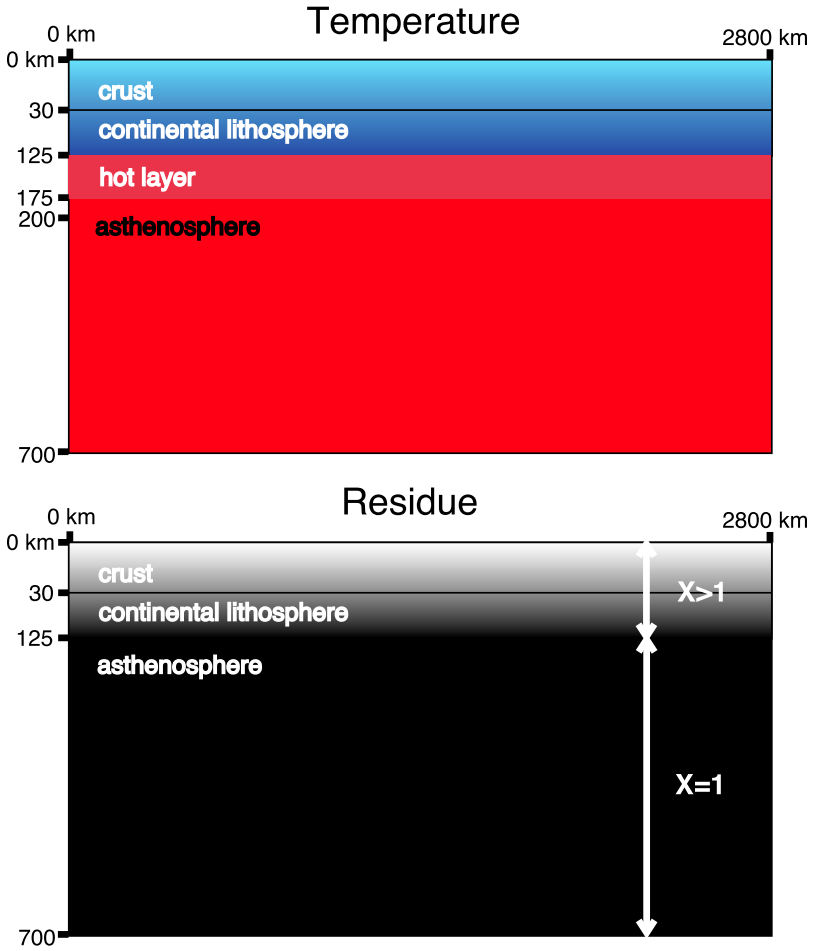

Figure 4. Initial condition for modeling the extension of the lithosphere, where the thermal anomaly is a layer of hot mantle beneath the lithosphere. The lithosphere is assumed not to have thinned prior to extension. (top) Initial temperature within the upper mantle, which includes the asthenosphere and lithosphere. The temperature at the base of the model at 700 km depth is either 1250, 1275 m or 1315°C. The 'hot layer' is either 0, 25, or 50 km thick and 100 or 200°C hotter than the mantle potential temperature. (bottom) Melt residue X for the upper mantle, where the lithosphere is melt depleted and therefore buoyant.

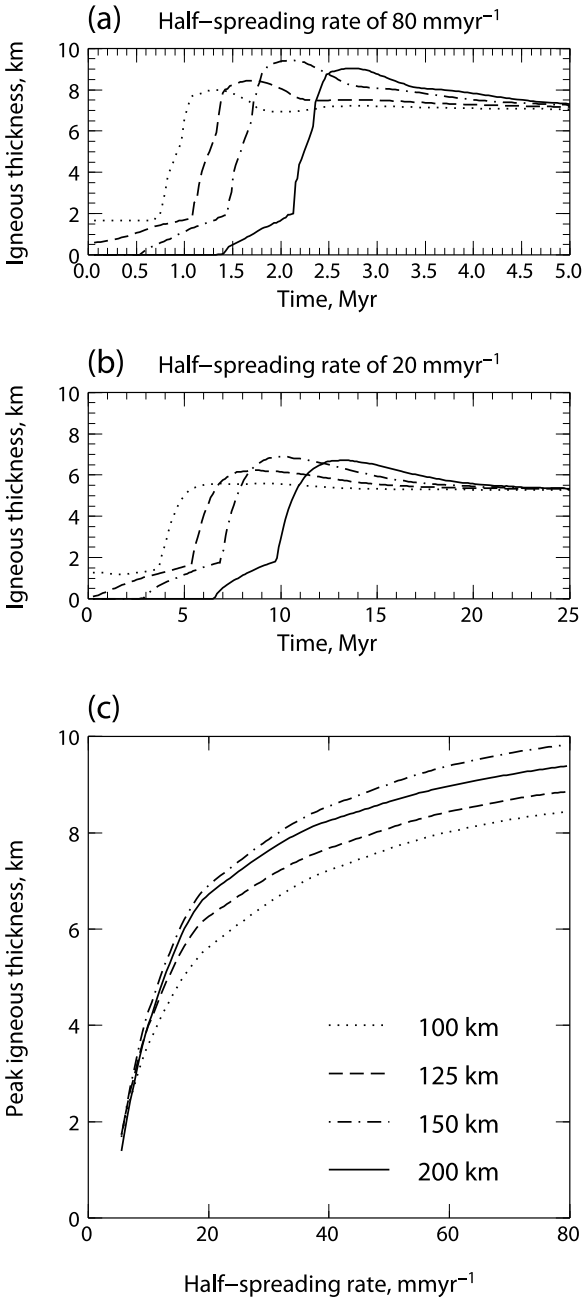

Figure 5. Igneous crustal thickness generated during extension of continental lithosphere of 100 to 200 km thickness with a 200°C, 50 km thick thermal anomaly. (a) Igneous thickness against time for extension at a half-spreading rate of 80 mm yr^{-1}. (b) As in Figure 5a for a half-spreading rate of 20 mm yr^{-1}. (c) Peak igneous thickness during breakup versus half-spreading rate. All plots are for four different initial lithosphere thickness, 100, 125, 150, and 200 km.

(Figure 4). The initial mantle temperature, which we vary between 1250 and 1315°C, is set at the base of the model and is held fixed at this temperature through time. The surface is held at a temperature of 0°C. The initial temperature profile is constant until the base of the lithosphere, at between 200 and 100 km, and then decreases linearly to 0°C. At the sides the temperature gradient is zero. Velocity boundary conditions are of free slip on the base and sides, and rifting is driven by a divergent velocity at the surface. The position of extension is defined by the fixed divergent velocity boundary condition. No prethinning is introduced [*Armitage et al.*, 2010]. In these viscous models of extension, we take melt generation as a proxy for the onset of extensional volcanism related to the rifting and eventual breakup. The finite element models have nodal resolution of 257 by 257. Extensive testing of the version of Citcom employed here has found that it is capable of accurately recreating rift evolution and melt generation at this resolution [*Nielsen and Hopper*, 2004]. We assume the bulk mantle composition is 49% primitive mantle and 51% MORB-like composition [*McKenzie and O'Nions*, 1991; *White and McKenzie*, 1995].

[12] The thickness of Indian continental lithosphere prior to the breakup of the India from the Seychelles is uncertain. Global models of the thermal thickness of continental lithosphere suggest Indian lithosphere is between 200 and 160 km thick [*Artemieva and Mooney*, 2001; *Priestly and McKenzie*, 2006]. However, a more recent regional study has suggested that present-day Indian continental lithosphere is around 100 km thick, and it is suggested that the Indian continental lithosphere was eroded during the 130 Ma breakup of the Permian Gondwanaland assemblage [*Kumar et al.*, 2007].

[13] In the absence of a thermal anomaly, extension of thicker lithosphere takes longer to reach the final constant oceanic crustal thickness of 7 km than for thinner lithosphere. However, if a thermal anomaly is present below the lithosphere more or less melt can be generated depending on the lithosphere thickness and temperature of the thermal anomaly (Figure 5). For a 50 km, 200°C hot layer beneath thick (>100 km) lithosphere a large proportion of the hot material will melt as the lithosphere thins and the hot mantle rock upwells (Figures 5a and 5b). If the lithosphere is very thick (>200 km), under the assumption that it is not replenished, hot mantle beneath the lithosphere will cool by thermal diffusion before the lithosphere lid thins to an amount sufficient to induce decompression melting. In the case of a 200°C, 50 km thick thermal anomaly the peak igneous thickness during breakup reaches a maximum for a lithosphere thickness of ~150 km (Figure 5c). The variation in thickness of igneous crust generated due to a 100 km variation in initial

Table 2. Partition Coefficients and Mantle Initial Compositions Used for Rare Earth Composition Calculations[a]

	La	Ce	Pr	Nd	Sm	Eu	Gd
Depleted Mantle	0.206	0.722	0.143	0.815	0.299	0.115	0.419
Primitive Mantle	0.55	1.40	0.22	1.08	0.35	0.13	0.457
Deccan Mantle	0.376	1.054	0.181	0.945	0.324	0.122	0.438
$\mathcal{D}_{ol}$	0.0035	0.0036	0.0003	0.005	0.006	0.010	0.0041
$\mathcal{D}_{opx}$	0.007	0.004	0.0095	0.0114	0.023	0.025	0.025
$\mathcal{D}_{cpx}$	0.12	0.17	0.07	0.31	0.49	0.48	0.59
$\mathcal{D}_{plag}$	0.10	0.072	0.10	0.050	0.036	0.26	0.030
$\mathcal{D}_{spinel}$	0.01	0.01	0.01	0.01	0.01	0.01	0.01
$\mathcal{D}_{garnet}$	0.012	0.21	0.034	0.07	0.36	0.5	0.7
	Tb	Dy	Ho	Er	Tm	Yb	Lu
Depleted Mantle	0.077	0.525	0.12	0.347	0.054	0.347	0.054
Primitive Mantle	0.084	0.57	0.13	0.372	0.058	0.372	0.057
Deccan Mantle	0.080	0.547	0.125	0.359	0.056	0.359	0.055
$\mathcal{D}_{ol}$	0.008	0.013	0.010	0.022	0.04	0.026	0.041
$\mathcal{D}_{opx}$	0.055	0.08	0.16	0.15	0.34	0.08	0.2
$\mathcal{D}_{cpx}$	0.64	0.70	0.66	0.68	0.8	0.62	0.60
$\mathcal{D}_{plag}$	0.028	0.022	0.011	0.04	0.036	0.013	0.015
$\mathcal{D}_{spinel}$	0.01	0.01	0.01	0.01	0.01	0.01	0.01
$\mathcal{D}_{garnet}$	1.10	2.7	3.6	3.3	3.0	5.7	6.2

[a]For each mineral and each rare earth, a partition coefficient has been estimated mainly from the database of *Torres-Alvarado et al.* [2003], with the exception of the spinel facies and Tm in garnet, which are from *McKenzie and O'Nions* [1991] and Tm in olivine, which is from *Frey* [1969]. The initial mantle compositions are from *McKenzie and O'Nions* [1991] and for the Deccan the source composition is that estimated for the Ambenali Formation by *White and McKenzie* [1995].

lithosphere thickness is up to 1.5 km (Figure 5). We are primarily interested in exploring the age constraints between the formation of the Gop Rift and eventual formation of oceanic crust, rather than the initiation of extension and breakup of the Permian Gondwanaland. Because there is evidence for a thinning Indian continental lithosphere since 130 Ma and the region of the Deccan Traps is cross cut by extensional basins, such as the Cambay Basin [*Dixit et al.*, 2010], we assume an initial lithosphere thickness of 125 km, noting that this assumption could lead to an under/over estimate of Gop Rift igneous crustal thickness of ±0.75 km.

2.3. Geochemistry

[14] We calculate the major and rare earth element (REE) composition of the melt generated. The melt composition is calculated from the melt fraction, temperature and pressure within the melt region by assuming incremental batch melting (see Appendix B). The major element composition is calculated using the methods of *Armitage et al.* [2009] and *Armitage et al.* [2010]. Following *Dean et al.* [2008], the REE melt composition is parameterized using the methods of *McKenzie and O'Nions* [1991] and the data sets of *Frey* [1969], *McKenzie and O'Nions* [1991] and *Torres-Alvarado et al.* [2003] (Table 2).

[15] The major and REE compositions are tracked as the rift scenarios evolve. We then calculate the mean melt composition over the whole melt region, following *McKenzie and Bickle* [1988],

$$\overline{C}_i = \frac{\int\int_{melt} FC dx dz}{\int\int_{melt} F dx dz}. \quad (12)$$

[16] To validate our melting model, we assume that melting of depleted mantle should produce normal MORB-like compositions at steady state. We have compared our models, where the half-spreading rate is 60 mm yr^{-1}, to MORB compositions from the East Pacific Rise (EPR), the Carlsberg Ridge in the Indian Ocean and the Mid-Atlantic Ridge (MAR; Figure 6). The model is in reasonable agreement with the observed REE pattern. For a mantle potential temperature of 1275°C the light REE (LREE) show a depletion that is similar to that of EPR basalts. For a hotter potential temperature, the LREE depletion is closer to that of the Carlsberg Ridge and MAR basalts. For the heavy REE (HREE), we find that our model predicts slightly more depletion than is expected. Overall the model appears to perform well for steady state seafloor spreading.

2.4. Seismic Velocities

[17] The prediction of major element composition of the melt allows the seismic velocity of the oceanic crust and underplate to be estimated. Here we use the relationship derived by *Behn and Kelemen*

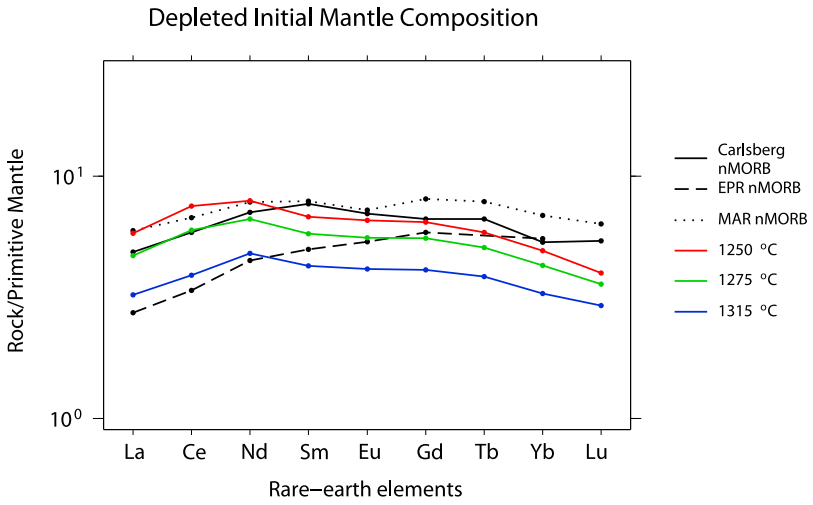

Figure 6. Predicted REE composition normalized to the primitive mantle of *Sun and McDonough* [1989] at steady state for a mantle temperature beneath the lithosphere of 1250, 1275, and 1315°C and half-spreading rates of 60 mm yr^{-1}. Predictions are compared to normal MORB from the Carlsberg Ridge at 6°N [*Rehkamper and Hofmann*, 1997], the East Pacific Rise (EPR), and Mid-Atlantic Ridge (MAR) [*Klein*, 2004].

[2003] using a 7 oxide system: SiO_2, Al_2O_3, MgO, FeO* (FeO + $0.9Fe_2O_3$), CaO, Na_2O and K_2O. By using the crystallization algorithm *Perple_X* [*Connelly*, 1990], the mineral data set of *Holland and Powell* [1998] and the elastic moduli data set of *Sobolev and Babeyko* [1994] they derive the following relationship,

$$V_p = 6.90 - 0.011 wt\%SiO_2 + 0.037 wt\%MgO + 0.045 wt\%CaO \quad (13)$$

for rocks within the depth range from 5 to 50 km, with stated uncertainties of ±0.13 km s^{-1} [*Behn and Kelemen*, 2003]. CaO is included in this relationship because *Behn and Kelemen* [2003] include the garnet phase. This parametrization does not include further major elements, because the inclusion of other elements did not improve the fit of their linear regression of calculated V_p [*Behn and Kelemen*, 2003]. Given the uncertainties involved in these calculations we assume the same depth of crystallization for both underplate and oceanic crust.

3. Results

[18] Oceanic crust adjacent to the Seychelles-Laxmi margin is about 25% thinner than the global average [*Collier et al.*, 2009]. Three possible explanations for the crustal thickness will be explored, as follows.

[19] 1. The mantle was abnormally cool at the time of rifting and onset of seafloor spreading. We investigate the possibility that the asthenospheric mantle was at the cooler end of the range of reasonable temperatures by modeling rift evolution with mantle potential temperatures of 1250, 1275 or 1315°C.

[20] 2. The high melt production that led to the underplating and thickened oceanic crust under the Gop Rift depleted the mantle to such an extent that when the center of extension shifted into the Seychelles-Laxmi region, the mantle was less fertile. To simulate such a scenario we alter the solidus depletion gradient, $(\partial T_s/\partial X)_z$, to values between for melting of a normal mantle and 800°C for melting of a depleted mantle.

[21] 3. The melting of the mantle during the opening of the Gop Rift dehydrated the mantle. If the mantle did not rehydrate, then when breakup occurred between Laxmi Ridge and the Seychelles the subsequent melting may be of a dry mantle. This would cause the melting region to reduce in size, as mantle that is volatile poor starts to melt at a shallower depth, which could have produced thin oceanic crust.

3.1. Individual Extensional Episodes

[22] First we will explore the evolution of the Gop Rift and Seychelles-Laxmi margins alone. This allows us to select the likely rift scenarios for the final combined simulation of the breakup of India and the Seychelles presented in section 3.2.

3.1.1. Gop Rift

[23] The formation of the Gop Rift resulted in the generation of significant volumes of melt [*Minshull*

Table 3. Possible Ages and Half-Spreading Rates for the Oceanic Crust Within the Gop Rift[a]

Reference	Chron	Approximate Age (Ma)	Half-Spreading Rate (mm yr^{-1})
Collier et al. [2008]	29r to 28r	65.5 to 64.5	26
Collier et al. [2008]	31r to 29r	70 to 65	6
Collier et al. [2008]	32n.1r to 31r	71.5 to 70.5	68
Yatheesh et al. [2009]	32r to 25r	71 to 56	5 (at breakup)
Yatheesh et al. [2009]	29r to 25r	65 to 56	30 (at breakup)

[a]For comparison, the main phase of the Deccan occurred within anomaly 29r, which is dated 65 ± 1 Ma [*Courtillot and Renne*, 2003].

et al., 2008]. The igneous material is up to 12 km thick and thins to 9 km. It formed approximately 1000 km to the west of the possible Deccan thermal anomaly (see Figure 1), opened either prior to, or is synchronous with the formation of the Deccan flood basalts, and it extended at different spreading rates (Table 3, scenarios 1 to 3 [*Collier et al.*, 2008]). REE element inversions suggest that the Deccan thermal anomaly was between 100 and 200°C hotter than background mantle potential temperature [*White and McKenzie*, 1995]. According to the plume model, the thickness of the hot layer that spread out beneath the lithosphere is dependent on the shape of its base and flux of hot material delivered from the thermal plume [*Sleep*, 1996]. We assume the plume has spread laterally such that its thickness is 50 km, as modeled at the Southeast Greenland margin at a similar lateral distance from the Iceland plume at the time of rifting [*Nielsen and Hopper*, 2004; *Armitage et al.*, 2008] (see Figure 4). We also test the effect of assuming a thinner hot layer of 25 km thickness corresponding to a 16-fold reduction in plume flux [*Ribe and Christensen*, 1994; *Sleep*, 1996]. We assume that at the start of the model run that there is no sublithospheric topography.

[24] Simulations of the extension that formed the Gop Rift show that spreading rates must have significantly exceeded 5 mm yr^{-1} to produce excess magmatism (Figure 7). The thermal anomaly also was likely at least 50 km thick, as we find for a 25 km thick thermal anomaly that melt generation during early extension is only slightly elevated above that without any anomaly (Figure 8). If the thermal anomaly was just 100°C then the lower crustal seismic velocities during early extension do not provide a good match to the trend of observations for both background mantle temperatures (Figures 7c and 7d). For spreading rates of 80 mm yr^{-1} and a 50 km thick thermal anomaly of 200°C both trends in igneous thickness and lower crustal seismic velocity are better matched (Figures 7a and 7b).

[25] The comparison of igneous thickness observations to modeled thickness favor a background mantle temperature below the lithosphere of 1275°C during the formation of the Gop Rift. But given the uncertainties involved, these models cannot distinguish between the two tested half-spreading rates of 20 and 80 mm yr^{-1}. Both these spreading rates produce thicknesses of igneous material that are in general agreement with the measured igneous thickness. If the Gop Rift opened with half-spreading rates of ~80 mm yr^{-1}, then it formed prior to the extrusion of the Deccan flood basalts (Table 3). Opening with half-spreading rates of ~20 mm yr^{-1} would suggest that the Gop Rift was synchronous with the Deccan flood basalts. To differentiate between these two models we later model the combined evolution of the Gop Rift and Seychelles-Laxmi Ridge margins.

3.1.2. Seychelles-Laxmi Ridge Margins

[26] The Seychelles-Laxmi Ridge margins show little signs of excess volcanics. There are a few seaward dipping reflector series, yet at 5.2 km the oceanic crust is anomalously thin [*Minshull et al.*, 2008; *Collier et al.*, 2009]. Unlike the Gop Rift, there is a long, unbroken seafloor spreading sequence allowing for robust determination of rates and ages. From magnetic anomaly modeling it has been shown that the Seychelles-Laxmi margin opened with half-spreading rates of 60 mm yr^{-1} [*Collier et al.*, 2008]. The first step we take is to model the Seychelles-Laxmi Ridge forming independently of the Gop Rift, to assess what controlling factors in the model would cause reasonable reductions in crustal thickness from the global average of ~7 km [*Bown and White*, 1994]. The initial conditions are as in Figure 4 but without the thermal anomaly. Again we assume that at the start of the model run that there is no sublithospheric topography.

[27] The first factor is a reduction in background mantle temperature. To match the global average thickness, for our models, we find a mantle tem-

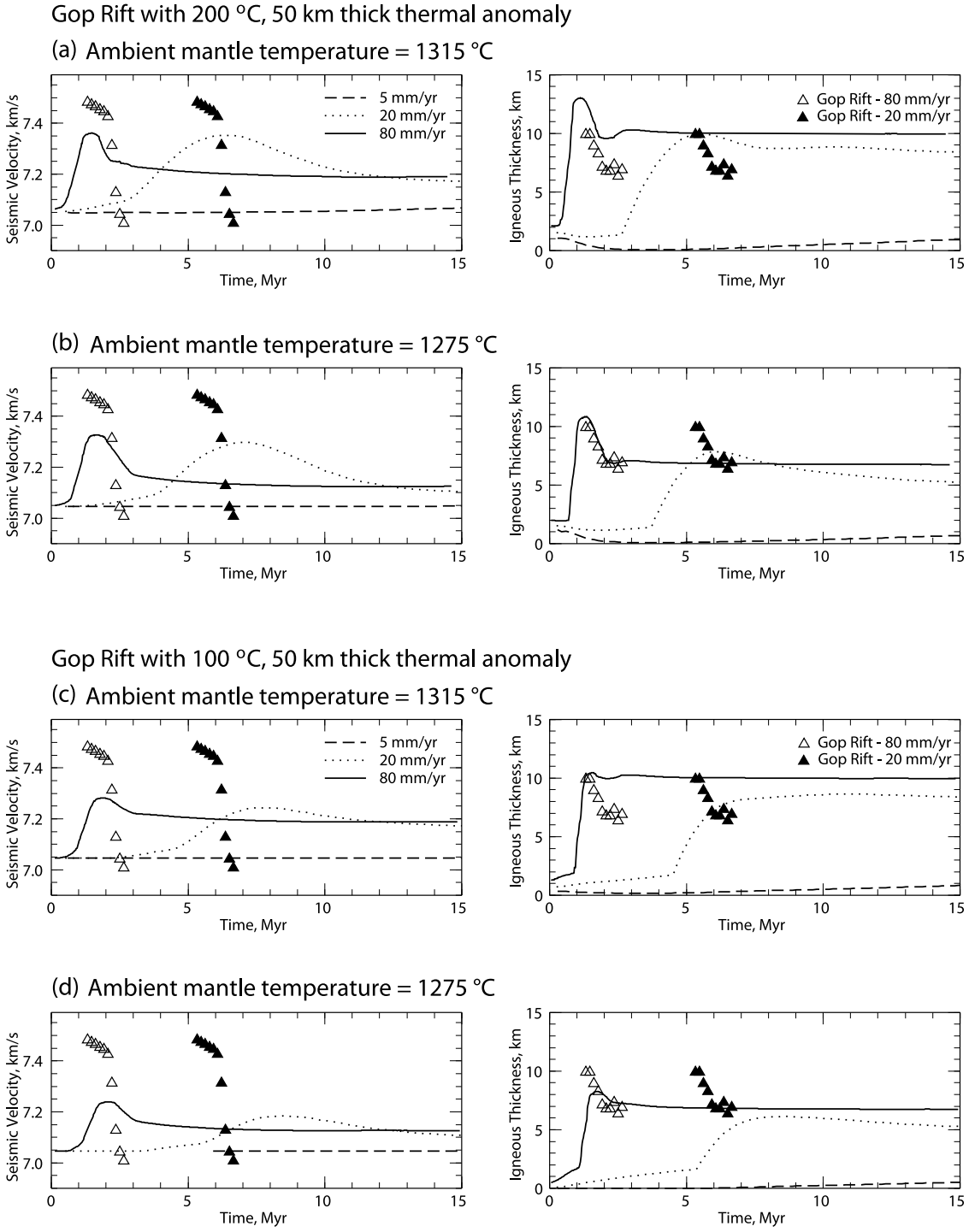

Figure 7. Seismic velocity and igneous crustal thickness (equation (11)) from simulations of the Gop Rift. (a) Seismic velocity of the lower crust and igneous crustal thickness during extension where the background mantle temperature beneath the lithosphere is 1315°C, and additionally there is a thermal anomaly of 200°C and 50 km thick. Half-spreading rates are 5, 20, or 80 mm yr^{-1}. Predicted seismic velocity and igneous thickness (lines) are compared to observations (triangles, Figure 2) [*Minshull et al.*, 2008] that are temporally matched to extension at 80 mm yr^{-1} (open triangles) and extension at 20 mm yr^{-1} (black triangles). (b) As in Figure 7a but the mantle temperature is 1275°C and the thermal anomaly is 200°C and 50 km thick. (c) As in Figure 7b but the mantle temperature is 1315°C and the thermal anomaly is 100°C and 50 km thick. (d) As in Figure 7c but the mantle temperature is 1275°C and the thermal anomaly is 100°C and 50 km thick.

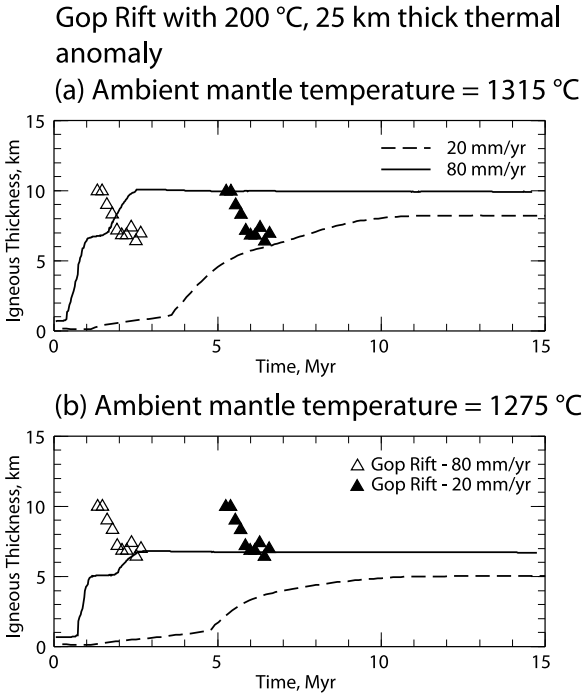

Figure 8. Igneous crustal thickness for a 200°C and 25 km thick thermal anomaly. (a) Igneous crustal thickness during extension where the mantle beneath the lithosphere is 1315°C. Half-spreading rates are 20 or 80 mm yr^{-1}. Predicted igneous thickness (lines) are compared to observations (triangles, Figure 2) [*Minshull et al.*, 2008] that are temporally matched to extension at 80 mm yr^{-1} (open triangles) and extension at 20 mm yr^{-1} (black triangles). (b) As in Figure 8a but the background mantle temperature is 1275°C.

perature beneath the lithosphere of 1275°C is required. Within our models we therefore assume that a mantle potential temperature of 1275°C is *normal*. For seafloor spreading at a half-spreading rate of 60 mm yr^{-1}, the mantle potential temperature would have to be reduced by 25°C to match the observed thinner crust (Figure 9a).

[28] Rather than the mantle cooling, the mantle beneath the Seychelles may have become depleted and dehydrated due to the prior extensional events that formed the Gop Rift. Similarly any plume material that lay under the lithosphere may also have become depleted and dehydrated due to the formation of the Gop Rift. To explore the consequences of these scenarios we simulated the formation of the Seychelles-Laxmi Ridge where the mantle is dehydrated (Figure 9b) and then included the effect of increasing the solidus depletion gradient of both the wet and dry solidus from 300 to 600 and 800°C (Figures 9c and 9d). If the mantle were considerably melt depleted, then we would expect it to be completely dehydrated. However, the timescale for the mantle to rehydrate is not well constrained.

[29] If the mantle is wet then melting begins at greater pressures (Figure 3) [*Hirth and Kohlstedt*, 1996]. Consequently the melt region stretches over a deeper and wider region. If the mantle is dry then this deeper region of the lithosphere will not melt and the predicted igneous crustal thickness is reduced by ~1 km (Figure 9b). Increasing the solidus depletion gradient likewise causes a reduction in igneous crustal thickness and seismic velocities, because of decreased fertility. Extension of the lithosphere above a very depleted mantle, that has been melted to such a degree that the solidus depletion gradient is 800°C, would reduce the crustal thickness generated by melting of a mantle of background temperature of 1275°C to 4.2 km (Figure 9c). If the mantle were both dry and very melt depleted then the igneous crustal thickness would be further reduced to 3.2 km (Figure 9d), which is less than that observed.

[30] Therefore, there are two possibilities to explain the thin crust; that the mantle cooled after the formation of the Gop Rift (dashed line, Figure 9a), or that the mantle became mildly depleted and not entirely dehydrated (dashed line, Figure 9c). Both of these scenarios are in agreement with the observed seismic velocities.

3.1.3. Seychelles: Rare Earth Elements

[31] The observed REE composition of three dredged seamounts off the northern Seychelles plateau appear to lie on a trend between the Ambenali Formations from the Deccan and that of normal MORB produced at the modern Carlsberg Ridge [*Collier et al.*, 2008]. Therefore, there may be a component of the Deccan source within these early oceanic crustal samples.

[32] The steady state solution of our simulation of the formation of the Seychelles-Laxmi Ridge margins is representative of seafloor spreading, and as such the REE composition of the melts generated at steady state is close to the normal MORB composition (Figure 6). We now apply the model to try to understand the flat REE profile of basalts from the foot of the Seychelles plateau (Figure 10). Samples from dredge 3 have an age of ~60 Ma from $^{40}Ar/^{39}Ar$ dating and so these rocks were emplaced 3 to 4 Myr after breakup had occurred

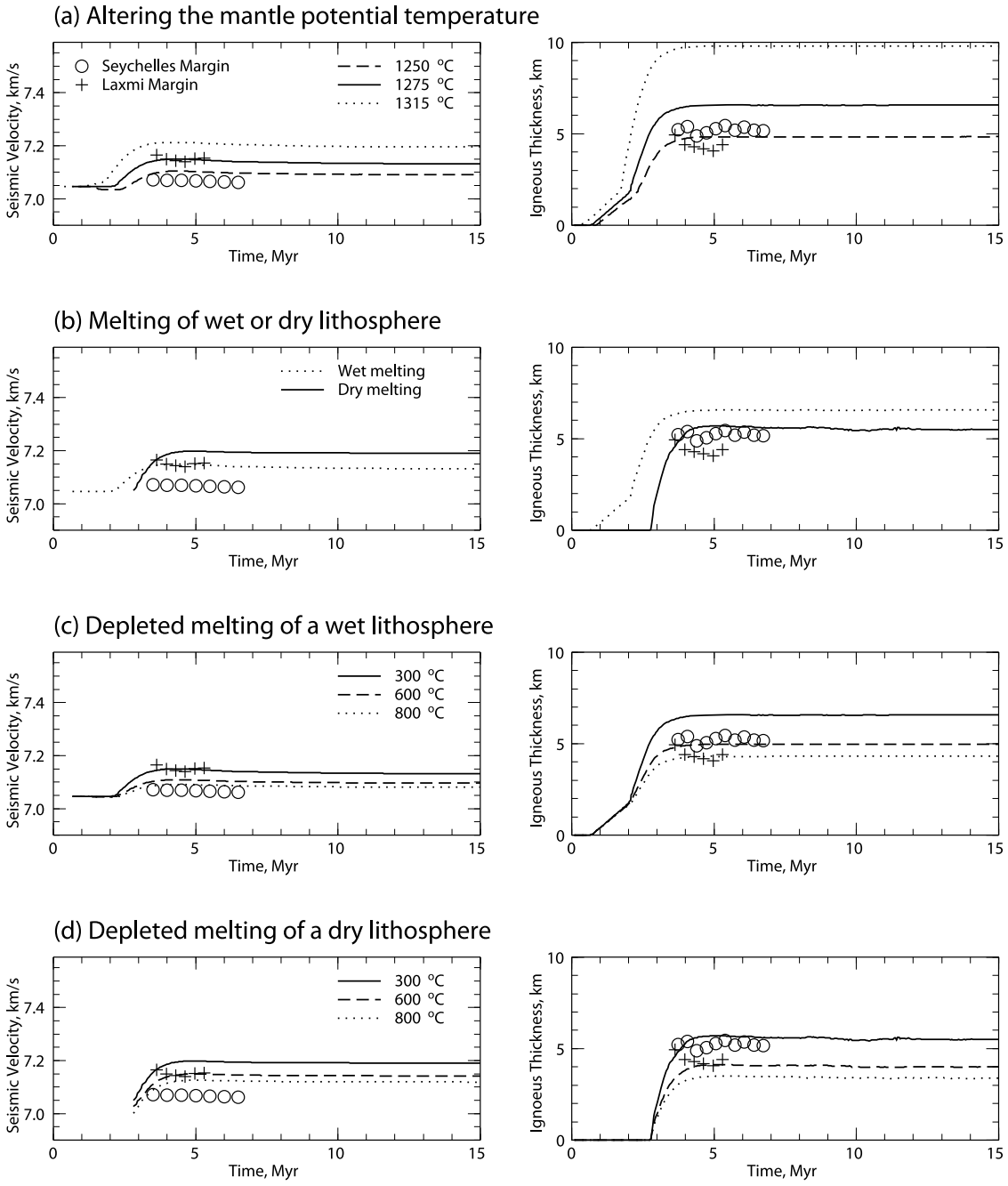

Figure 9. Seismic velocity and igneous crustal thickness (equation (11)) from simulations of the Seychelles-Laxmi Ridge margins. The half-spreading rate is 60 mm yr^{-1}. (a) Seismic velocity of the lower crust and igneous crustal thickness during extension, where the mantle beneath the lithosphere is either 1250, 1275, and 1315°C. The circles and crosses mark the observed lower crustal seismic velocities and igneous thickness at the Seychelles and Laxmi Ridges, respectively [*Collier et al.*, 2009], matched to model breakup time. (b) Seismic velocity and igneous crustal thickness during extension for mantle temperature of 1275°C, where the mantle is pristine (wet melting) or dehydrated (dry melting). (c) Seismic velocity and igneous crustal thickness during extension for mantle of a temperature of 1275°C, where the solidus depletion gradient (equation (9)) is either 300 (not depleted), 600 (mildly depleted), or 800°C (very depleted). (d) As in Figure 9c but the mantle is dehydrated.

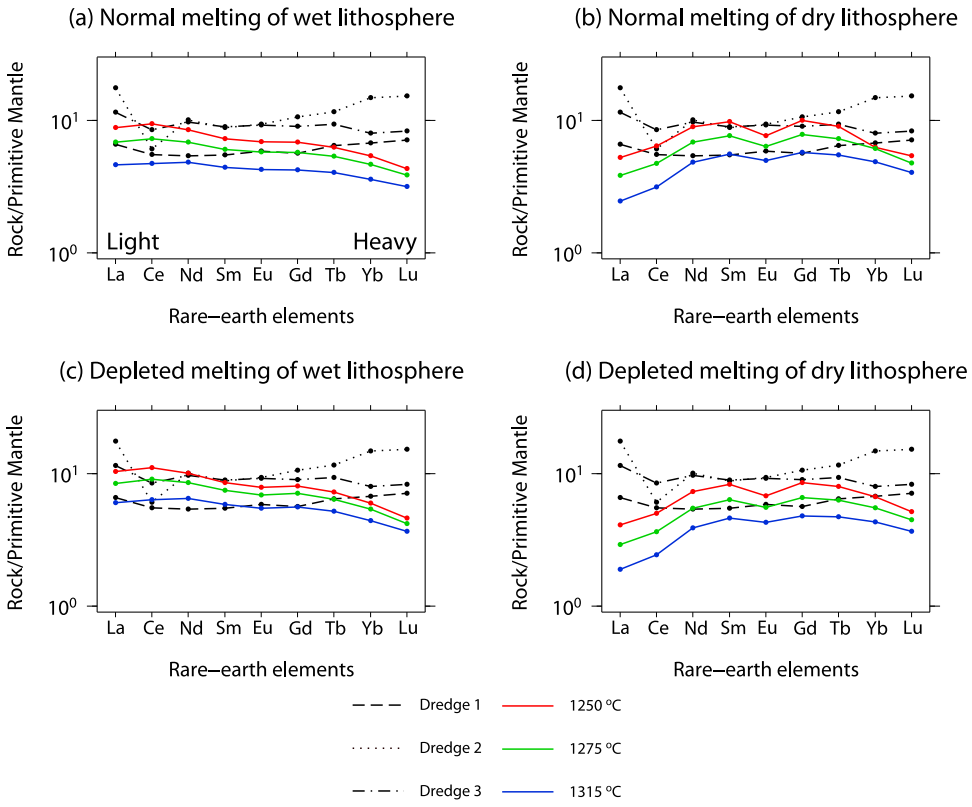

Figure 10. Predicted (colored lines) and observed (black lines) REE compositions at the Seychelles margin. (a) The mantle beneath the lithosphere is of 1250, 1275, and 1315°C, with a solidus depletion gradient of 300°C. (b) Melting of a dehydrated mantle with a solidus depletion gradient of 300°C. (c) Melting of depleted mantle with a solidus depletion gradient of 600°C. (d) Melting of a depleted and dehydrated mantle with a solidus depletion gradient of 600°C. Predictions are compared to analysis of dredge samples from the northern Seychelles margin [*Collier et al.*, 2008]. The locations of these dredges are shown in Figure 2.

[*Collier et al.*, 2008]. We compare REE compositions of the dredge samples with those predicted 6 Myr after initiation of extension within the model, once steady state oceanic crustal thickness is achieved.

[33] For melting of a Deccan-like mantle (see Table 2) the predicted REE composition for all plausible mantle potential temperatures is too depleted in the HREE when compared to the Seychelles dredge samples (Figure 10a). Earlier we suggested that the anomalously thin oceanic crust may be due to melting of a depleted and dehydrated mantle or a cooler mantle. To further assess the consequences of these scenarios, we compare predicted REE compositions to the dredge samples. Increasing the depletion solidus gradient, to simulate melting of a depleted mantle has the effect of enriching both LREE and to a lesser extent HREEs (Figure 10c). The effect of assuming a dehydrated mantle is to slightly enrich the HREE and deplete the LREE (Figures 10b and 10d).There is also a slight depletion of Eu from melting above a dry mantle, as there is a greater proportion of melt that forms feldspars (melting in the plagioclase stability field).

[34] The increase in seismic velocities predicted from the major element compositions suggested that melting of a dehydrated mantle is unlikely to be the cause of the thin crust off the Seychelles (Figure 9). Likewise, the REE composition predictions also suggest that melting of a dehydrated mantle is unlikely. As was the case for our modeling of normal MORB (Figure 6), we find that our model predictions in general overestimate the depletion of the HREE. We conclude that the cause of the thin crust offshore Seychelles is either melting of a depleted mantle or a drop in mantle temperatures. We will now apply these two concepts to a combined model of the formation of both the Gop Rift and the Seychelles-Laxmi Ridge margin.

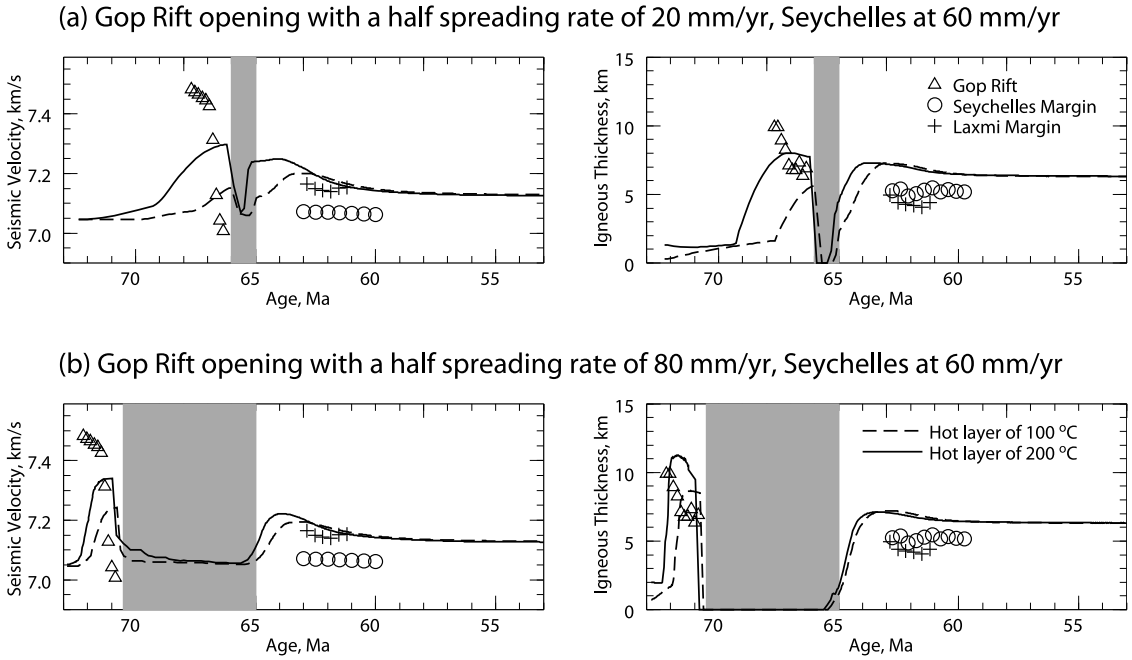

Figure 11. Seismic velocity of the lower crust and igneous crustal thickness for the evolving northwest Indian Ocean. (a) The Gop Rift forms at a half-spreading rate of 20 mm yr^{-1} at ~67 Ma. This is followed by the formation of the Seychelles-Laxmi Ridge margin at 65 Ma. The grey shaded region marks the time interval between the two episodes when there is no extension. The triangles, circles, and crosses mark the observed seismic velocity and crustal thickness at both margins [*Minshull et al.*, 2008; *Collier et al.*, 2009]. (b) As in Figure 11a but the Gop Rift forms at a half-spreading rate of 80 mm yr^{-1} at 71 Ma.

3.2. Multiphase Extension

[35] Our modeling of the Gop Rift presented in section 3.1.1 has shown that the thermal anomaly beneath the Gop Rift was ~200°C, half-spreading rates were at least 20 mm yr^{-1}, and the background mantle temperature below the lithosphere was greater than 1250°C. Our modeling of the Seychelles-Laxmi Ridge margin, presented in section 3.1.2, has shown that the mantle temperature was less than 1315°C, and that the mantle may have been depleted when the margin formed. In this section, we model the evolution of the two margins combined. We wish to understand the connection between the thick crust of the Gop Rift and the thin oceanic crust formed by the young Carlseberg Ridge, and to better constrain the ages of the events that resulted in the breakup between the Seychelles and India.

[36] We explore the two scenarios of the evolution of the northwest Indian Ocean determined by magnetic anomaly modeling [*Collier et al.*, 2008] that are compatible with the modeling work presented in section 3.1. The first scenario is that within the Gop Rift seafloor spreading began at around 66 Ma, at a half-spreading rate of ~20 mm yr^{-1}, and was quickly (1 Myr) followed by the seafloor spreading between the Seychelles-Laxmi Ridge margins at a half-spreading rate of 60 mm yr^{-1}. The second scenario is that seafloor spreading within the Gop Rift began at around 71 Ma, at a half-spreading rate of ~80 mm yr^{-1} and, after 8 Myr, was followed by seafloor spreading between the Seychelles-Laxmi Ridge margins at a half-spreading rate of 60 mm yr^{-1}. Our work presented in section 3.1.2 showed that any thermal anomaly must be exhausted or cool significantly prior to the formation of the Seychelles-Laxmi Ridge margins.

[37] Building on our analysis in section 3.1 we assume that the mantle temperature beneath the lithosphere was a little cooler than the suggested global temperature of 1315°C [*McKenzie et al.*, 2005], and model the combined rift evolution with a mantle temperature of 1275°C. We begin with the initial conditions as Figure 4 with no prethinning of the lithosphere as in sections 3.1.1 and 3.1.2. The Gop Rift is first simulated by imposing extension at a half-spreading rate of 20 or 80 mm yr^{-1}. The lithosphere cools and thickens due to thermal diffusion for 1 or 8 Myr before the center of extension migrates south of the Laxmi Ridge and extension is imposed between the Laxmi Ridge and Seychelles.

[38] The results of the combined modeling of the two margins are shown in Figure 11. If the formation

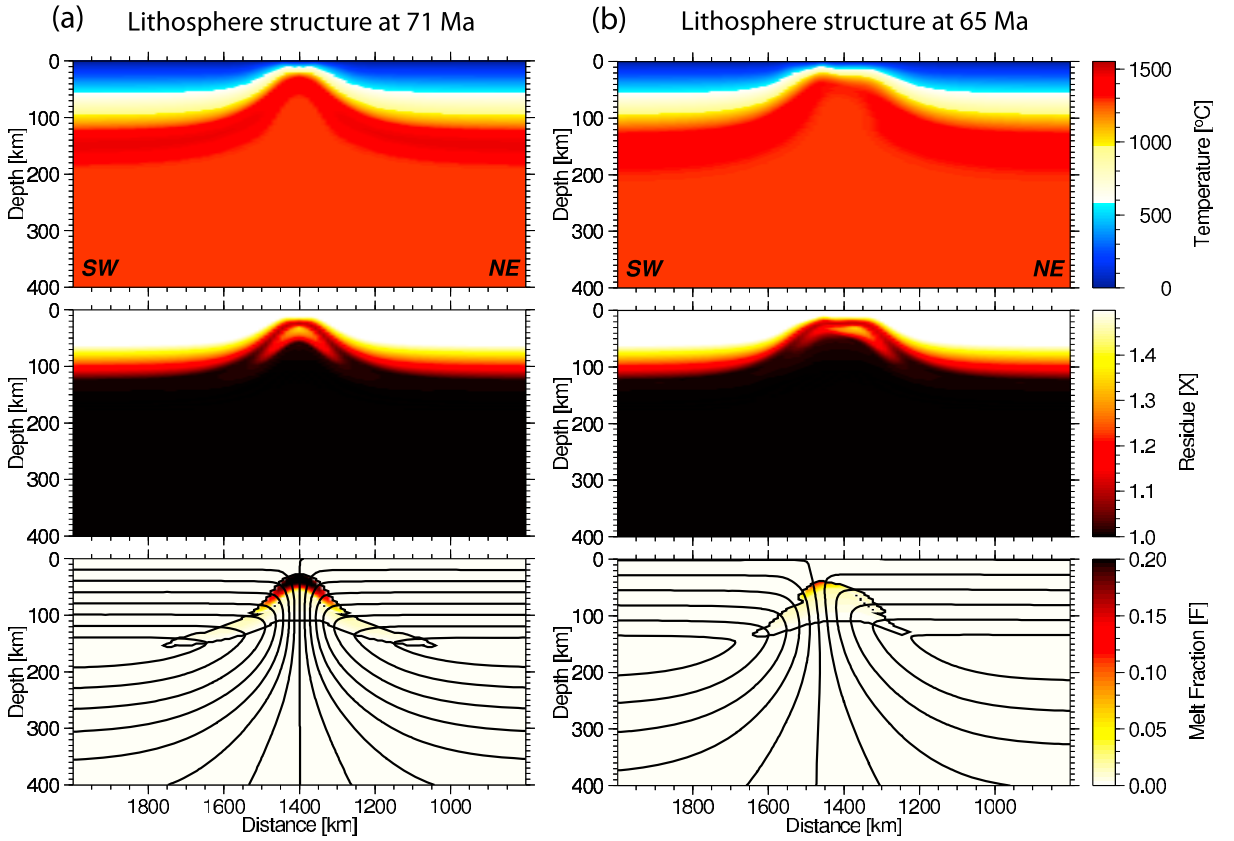

Figure 12. Structure of the lithosphere and mantle for our preferred model. (a) Structure during the formation of the Gop Rift at a half-spreading rate of 80 mm yr^{-1}. The mantle temperature beneath the extending lithosphere is 1275°C, and the thermal anomaly is initially 50 km thick and 200°C. (top row) Temperature, (middle row) melt depletion (see equation (5)), and (bottom row) melt fraction and streamlines of flow. (b) Structure during the initial formation of the Seychelles-Laxmi Ridge margins at a half-spreading rate of 60 mm yr^{-1}.

of the Gop Rift was synchronous with the Deccan flood basalts, then there is a very short, 1 Myr period of time during which the center of extension migrated southward of the Laxmi Ridge. The igneous crustal thickness generated in this scenario is too thin when compared to the observations at the Gop Rift and too thick for the later oceanic crust (Figure 11a). Instead, if the two episodes of extension were separated by 8 Myr, for a 200°C thermal anomaly, the igneous crustal thickness of the Gop Rift is reproduced, but the crustal thickness between the Seychelles and Laxmi Ridge is still too high, between 7 and 6 km (Figure 11b, solid line). This is because in both scenarios the thermal anomaly has not cooled sufficiently. Reducing the thermal anomaly to 100°C degrades the fit to the Gop Rift observations without significantly improving the fit to the Seychelles-Laxmi Ridge observations (Figure 11, dashed lines)

[39] The formation of the Gop Rift left behind a region of depleted mantle (Figure 12a). Despite the migration of extension southwest of the Laxmi Ridge, the mantle remains depleted (Figure 12b). Unfortunately, our model is unable to track individual points in the residual mantle with different melting characteristics. However, as in section 3.1.2, we can assume that the mantle melted during the formation of the Seychelles-Laxmi Ridge margin is uniformly depleted. With an increase in the solidus depletion gradient to 600°C, the modeled igneous crustal thickness for the Seychelles-Laxmi Ridge is reduced to 5 km, as observed, for both rift history scenarios (Figure 13).

[40] Thus our work shows that it is more likely that the Gop Rift was formed during a pre-Deccan period of extension for two reasons. Firstly, if the Gop Rift formed at very fast spreading rates (~80 mm yr^{-1}) then the observed crustal thickness and seismic velocity can be reconciled (Figure 13). Secondly, the increased time between phases of extension allows the mantle to cool by thermal diffusion.

[41] In summary, we infer the following: (1) the Gop Rift and Seychelles-Laxmi Ridge formed above

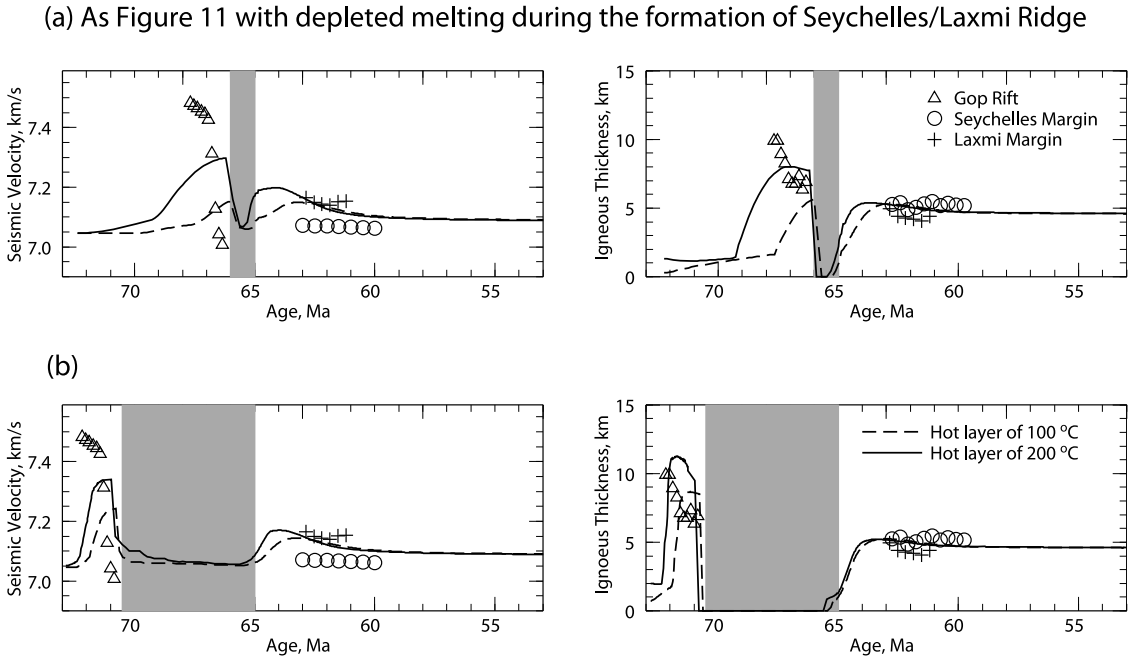

Figure 13. Seismic velocity of the lower crust, igneous crustal thickness for the evolving northwest Indian Ocean where the mantle becomes depleted. (a) The Gop Rift forms at a half-spreading rate of 20 mm yr^{-1} at ~67 Ma. This is then followed by the formation of the Seychelles-Laxmi Ridge margins at 65 Ma, where the mantle is depleted and the solidus depletion gradient is 600°C. (b) As Figure 13a but the Gop Rift forms at a half-spreading rate of 80 mm yr^{-1} at 71 Ma. The 200°C hot layer phase (solid line) is our best-fit model [*Armitage et al.*, 2010].

a mantle of 1275°C, (2) the Gop Rift formed above a ~200°C, 50 km thick thermal anomaly with a half-spreading rate of 80 mm yr^{-1} and opened at around 71 Myr, up to 4 Ma prior to the main phase of the Deccan flood basalts, and (3) the melting due to the thermal anomaly likely led to the depletion of the mantle prior to the extension and breakup of the Seychelles-Laxmi Ridge margin, leading to the observed thin, low seismic velocity oceanic crust and flat REE profile.

4. Discussion

4.1. Relative Timing of Extension and Flood Basalt Eruption

[42] Our modeling work presented here, together with our analysis of seismic [*Minshull et al.*, 2008; *Collier et al.*, 2009] and magnetic data [*Collier et al.*, 2008], suggests that the separation of the Seychelles from India occurred in two phases, one before and the other shortly after the eruption of the bulk of the Deccan flood basalts. Although an early phase of extension has been previously recognized in the Gop Rift/Laxmi Ridge area [*Bhattacharya et al.*, 1994; *Malod et al.*, 1997], most workers have to date only considered a single phase of extension leading up to the production of seafloor-spreading magnetic anomalies between the Seychelles and India. Our model shows that it is not possible to generate the oceanic crust observed across this region with a single rift event. A small degree of extension could have occurred in both regions prior to breakup and that would require protracted period of extension leading to eventual breakup between the Seychelles and Laxmi Ridge to match our preferred timings.

[43] The relative timing of the extension that culminated in the continental breakup of India and the Seychelles and the main tholeiitic phase of flood volcanism has been long debated in the case of the Deccan, and it is one of the key observations for understanding its causal mechanism [*Courtillot et al.*, 1999; *Sheth*, 2000]. The orientations of feeder dykes at various sites across the Deccan province, for example, have been previously interpreted to imply both pre-eruption and posteruption extension. *Kent et al.* [1992] argued that dykes in and around the Narmada Rift in the north of the province, that have been dated as 67–64 Ma [*Bhattacharji et al.*, 1996], show a strong east-west alignment indicating that extension here was underway before flood basalt eruption. They further argue that similarly oriented dykes, dated as 73–69 Ma [*Dickin et al.*, 1986], are also found in the Seychelles. The Gop

Rift is parallel to this trend, and so the extension and seafloor spreading recorded there is entirely consistent with the onshore strain pattern. Alternatively, *Hooper* [1990] and *Hooper et al.* [2010] dismiss the significance of this older alkaline series of east-west orientated dykes, and conclude that because a younger series of tholeiitic dykes to the south were randomly orientated extension must have occurred shortly after the main eruption event. Our model, with episodes of lithospheric extension either side of the onshore Deccan eruption resolves this controversy by suggesting that in fact both interpretations of the feeder dyke orientations may be correct.

[44] We cannot address the cause of rift migration within our model [see *Armitage et al.*, 2009]. In our study area the pattern of extension is 3-D in nature as extension propagated northward and we only have a single transect. This is particularly relevant as the continental blocks involved are comparatively small. Prior to the opening of the Gop Rift, the extension was taken up in the Mascarene basin, to the south of the Seychelles block (Figure 1). Unfortunately the identification of seafloor spreading anomalies in this basin has proved difficult, but *Bernard and Munschy* [2000] identify anomaly 32/33 to be the youngest anomalies in the north of the basin, which is entirely consistent with our geodynamically favored model of the Gop Rift opening during anomalies 31 and 32. This initial ridge jump is consistent with previous observations that the arrival of a mantle plume can lead to migration of spreading centers [*Jurine et al.*, 2005; *Mittelsteadt et al.*, 2008, 2011]. Migration of the spreading center toward the plume is dependent on the degree of heating produced by the presence of hot mantle at the base of the lithosphere, the generation of melt and propagation of that melt through the lithosphere, leading to weakening [*Mittelsteadt et al.*, 2008]. Migration is toward the plume, or if the degree if heating is low the plume may be captured by the spreading center [*Mittelsteadt et al.*, 2011]. However, during the time period of our study, seafloor spreading continued in the Mascarene basin, although it progressively retreated southward, with the youngest magnetic anomaly being found at its southern margin being 27, which is again consistent with the establishment of a south-eastward propagating Carlsberg Ridge to the north.

[45] Something that is more difficult to speculate on is why the Gop Rift, once established did not carry on to develop into an mature ocean basin. Extension above incubated hot mantle formed the underplate beneath the Gop Rift. Intruded melt in the crust can lead to weakening and the migration of the center of extension [e.g., *Corti et al.*, 2003; *Yamasaki and Gernigon*, 2009]. The numerical modeling study of *Yamasaki and Gernigon* [2010] suggests that it is possible that the migration of the center of the extension to the west of the Laxmi Ridge was a by product of the alteration of the strength of the lithosphere due to the intrusion of magmatic material. This proposed mechanism would require that extension was present in both the Gop Rift and Seychelles/Lamxi Ridge regions prior to breakup. In our model we impose two distinct extension events separated by 8 Myr, but we cannot rule out that extension prior to the significant production of melt could have occurred across the region.

4.2. Plume Incubation

[46] We have reproduced successfully our offshore geophysical observations with a numerical model in which a hot layer arrived beneath a thinning lithosphere in the Gop Rift area around 72 Ma. The origin of the Deccan flood basalts has been related to a possible mantle plume that has since migrated southwest ward forming the Chagos-Laccadive Ridge, Mascarene Ridge and Réunion Island [*Richards et al.*, 1989; *White and McKenzie*, 1989]. *Anderson* [1994] offers a counter suggestion, that edge-driven convection due to the variation in lithospheric thickness beneath the Indian subcontinent and the surrounding basins could cause decompression melting. However, the strength of edge-driven convection is highly dependent on the choice of rheology [*Korenaga et al.*, 2002]. Our modeling work is built upon that of *Nielsen and Hopper* [2004] who found that the convection that nucleated off the edge of 250 km thick continental lithosphere did not generate significant amounts of melt. Equally, edge-driven convection does not strongly nucleate during the inter-rift period within our model. The lack of vigorous edge-driven convection is in agreement with the scaling arguments of *Sleep* [2007]. It is therefore unlikely that edge-driven convection could provide the excess melt generation that would be necessary to explain the Deccan Traps and underplate observed in the Gop Rift.

[47] In order to match the temporal variation in the thickness and P wave seismic velocities of the melt produced, we require a hot layer that is comparable in terms of excess temperature (200°C) and dimensions (50 km thick at ~1000 km from the center of the associated flood basalt province) to that expected for a new mantle plume as it impacts and spreads out beneath the lithosphere [*Hill et al.*, 1992; *Cambell*,

2007]. Hence our work supports the plume incubation as opposed to the plume impact model, with a mantle thermal anomaly in place below western India at least 7 Ma before the main tholeiitic eruption. Interestingly, the age that we determine for the initiation of seafloor spreading in of the Gop Rift shortly postdates the 73.4 to 72.0 Ma age of the Bibai volcanics in the Tethyan suture zone of Pakistan that have been previously interpreted as representing an early phase of Réunion hot spot activity [*Mahoney et al.*, 2002]. Further evidence of volcanic activity on the periphery of Greater India (India and Seychelles) around this time comes from the presence of thick pillow lavas within Upper Cretaceous sediment in commercial drill holes on the southern Seychelles Plateau [*Plummer*, 1995]. We conclude that the pattern of volcanic activity at this early stage was not directly controlled by the location of the plume axis, but rather reflected areas of thin lithosphere as envisaged by *Thompson and Gibson* [1991] and *Ebinger and Sleep* [1998].

[48] An implication of the age of the Gop Rift magmatic extensional event is that there may have been significant pre-Deccan vertical uplift of western India. Recognizing such an event onshore is difficult and controversial due to the thick pile of volcanics and posteruption history [*Saunders et al.*, 2007]. Furthermore, the interaction of a plume head with continental lithosphere can lead to a complex pattern of uplift and subsidence [*Burov and Guillou-Frottier*, 2005]. However, perhaps the most convincing evidence of vertical uplift to date is the record of a significant increase in sediment depositional flux within deep offshore wells during the Late Campanian and Early Maastrichian (72 to 69 Ma [*Halkett et al.*, 2001]). This observation is consistent with the onset of seafloor spreading in the Gop Rift during this period. A ~71 Ma pre-Deccan event may also explain why previous analyses of apatite fission track data have been unable to detect distinct denudation signals due to the separation of Madagascar (at ~84 Ma) and the Seychelles (63.4 Ma) from India [*Gunnell et al.*, 2003]. The intermediate Gop Rift event would have blurred the temporal signal of these other two continental breakup events.

4.3. Cool Mantle Under the Indian Ocean?

[49] In comparison to the North Atlantic margins, a 50°C lower background mantle temperature in the northwest Indian Ocean is required to fit the later parts of the volcanic history and steady state crustal thickness, once the hot layer is exhausted [*Armitage et al.*, 2008, 2009]. This temperature difference of 50°C for the mantle potential temperature is not geodynamically significant other than decreasing overall melt production. Regional differences in mantle potential temperature of this magnitude may well be present naturally within the upper mantle worldwide [*Anderson*, 2000]. Alternatively, the hotter background asthenosphere in the Atlantic case may be due to continental insulation effects, with North America–Europe being stationary above the rising plume, whereas Greater India was moving rapidly northward at the time of plume impact (180–200 mm yr^{-1} during the late Cretaceous [*Gaina et al.*, 2007]).

5. Conclusions

[50] We have developed a geodynamic model of rift evolution that is capable of predicting oceanic crustal thickness, seismic velocity, and REE and major element melt compositions. We find that this model can reproduce the normal MORB REE and major element profiles [*Armitage et al.*, 2008]. Given that the model performs well for the steady state conditions, we have then applied the model to the anomalous rifting styles in the northwest Indian Ocean: the volcanic Gop Rift that is in close proximity to the Deccan flood basalts, which is followed by the apparently magma starved Seychelles-Laxmi Ridge margin [*Minshull et al.*, 2008; *Collier et al.*, 2008].

[51] The Gop Rift is a narrow volcanic rifted margin with significant underplating [*Minshull et al.*, 2008]. Unfortunately, as it is so narrow, magnetic anomaly modeling has been unable to date uniquely the formation of this rift. By using our geodynamic model of rift evolution, we were able to discriminate between models compatible with magmatic anomaly observations and find that seafloor spreading in the Gop Rift began at 71 Ma. The underplate is related to a thermal anomaly incubated under the Indian subcontinent. This thermal anomaly is likely from the Deccan thermal plume, which we suggest impacted the lithosphere up to 8 Myr prior to the eruption of the Deccan flood basalts. The plume spread laterally upon impact, and when the Gop Rift extended and rifted, at 71 Ma it tapped this hot mantle, causing excess melt production.

[52] After ~1 Myr of seafloor spreading extension at the Gop Rift ended. When extension migrated, 8 Myr later, the spreading center shifted southward, possibly due to the presence of weaker fragments

of continental lithosphere and the thermal anomaly had dissipated due to melting and cooling. The oceanic crust generated during the formation of the Seychelles-Laxmi Ridge margin is surprisingly thin. This reduced melt production is likely due to depletion of the mantle due to the earlier large melting event that formed the Gop Rift.

[53] It is clear that the factors that control rifting are complex, and that small changes in depletion and mantle temperature can cause dramatic changes in the melt production and subsequent crustal thickness. The Seychelles-Laxmi Ridge margin has previously been assumed to be magmatic as it is close to the Deccan flood basalts. We have however shown by resolving the age of formation of the Gop Rift that the mantle was likely depleted and despite the proximity of this margin to a possible thermal plume, thin oceanic crust could still be generated.

Appendix A: Melting Residue

[54] Following *Scott* [1992], the amount of melting is modeled using a completely compatible trace element, i.e., one that has a partition coefficient $D \rightarrow \infty$. This completely compatible element remains always within the solid as melting progresses. From *McKenzie* [1984], the mass balance for liquid, density ρ_l, and solid, ρ_s, are governed by

$$\frac{\partial}{\partial t}(\rho_l \phi) + \nabla \cdot (\rho_l \phi \mathbf{v}) = \frac{DM}{Dt} \tag{A1}$$

$$\frac{\partial}{\partial t}(\rho_s (1-\phi)) + \nabla \cdot (\rho_s (1-\phi)\mathbf{u}) = -\frac{DM}{Dt}. \tag{A2}$$

DM/Dt is the rate at which mass is transferred from the matrix to the melt, $\mathbf{v}$ and $\mathbf{u}$ are the liquid and solid velocities and ϕ is the porosity. From equation (A2), the solid composition C_s is given by the following conservation [*Spiegelman*, 1996],

$$\frac{\partial}{\partial t}(\rho_s (1-\phi) C_s) + \nabla \cdot (\rho_s (1-\phi)\mathbf{u} C_s) = -\frac{DM}{Dt}, \tag{A3}$$

and by substitution of equation (A2) into an expanded equation (A3) we get,

$$\frac{\partial C_s}{\partial t} + \mathbf{u} \cdot \nabla C_S = \left(1 - \frac{1}{D}\right) \frac{C_s}{\rho_s (1-\phi)} \frac{DM}{Dt}. \tag{A4}$$

Our equation (A4) matches with the completely compatible trace element concentration, X of *Scott* [1992], where the rate of mass transfer $DM/Dt = \rho_s \dot{m}$,

$$\frac{\partial X}{\partial t} + \mathbf{u} \cdot \nabla X = \frac{X}{1-\phi} \dot{m}, \tag{A5}$$

and $\dot{m}$ is the dimensionless melt production rate. In tensor notation this becomes

$$\frac{\partial X}{\partial t} = -u_i \frac{\partial X}{\partial x_i} + \frac{X}{1-\phi} \dot{m}. \tag{A6}$$

Appendix B

B1. Rare Earth Element Melt Composition

[55] The composition of an element, i, in the melt, l, is defined as from *Albarede* [1995]

$$C_{i,l} = \frac{m_{i,l}}{M_l}, \tag{B1}$$

and the melt fraction is

$$\mathcal{F} = \frac{M_l}{M_0}, \tag{B2}$$

where m is the mass of the element in the melt phase, M is the mass of the melt phase and M_0 is the initial mass. In order to calculate the composition of the melt, l, from the solid, s, composition we use the *bulk distribution coefficient*, as defined in the study by *Langmuir et al.* [1992]

$$D = \frac{C_{i,l}}{C_{i,s}}. \tag{B3}$$

[56] Mass conservation means that the initial mass of all phases is given by

$$M_0 = M_l + M_s, \tag{B4}$$

and the mass of each element in all phases is given by

$$m_0 = m_l + m_s. \tag{B5}$$

Within our model we assume that at each time step melt and solid matrix are in equilibrium with each other. Furthermore, following *Ito et al.* [1999], *Nielsen and Hopper* [2004] and *Armitage et al.* [2008], we make the simplifying assumption that all melt is extracted after each time step, where each time step is of the order of 40,000 years. Therefore, melt extraction is assumed to be faster than ~2 m yr^{-1} assuming that the deepest melts are formed at around 100 km, as modeled in the study by *Armitage et al.* [2008]. If melt extraction is by porous flow through the mantle matrix alone, then such an extraction velocity cannot be justified, but melt is likely removed more rapidly from the melt region by high-porosity channels [*Kelemen et al.*,

Table B1. Mineral Proportions, $P_{mineral}$, for the Calculation of Partition Coefficients, From *McKenzie and O'Nions* [1991]

	P_{Ol}	P_{Opx}	P_{Cpx}	P_{Plag}	P_{Spinel}	P_{Garnet}
Plagioclase peridotite	0.636	0.263	0.012	0.089	-	-
Spinel peridotite	0.578	0.270	0.119	-	0.033	-
Garnet peridotite	0.598	0.211	0.076	-	-	0.115

1997; *Holtzman et al.*, 2003; *Stracke et al.*, 2006]. Therefore, at each new time step, $n + 1$, the melt is generated from the solid residual from the previous time step, n,

$$M_s^n = M_l^{n+1} + M_s^{n+1} \tag{B6}$$

and

$$m_s^n = m_l^{n+1} + m_s^{n+1}. \tag{B7}$$

This is incremental batch melting, where at each time step the melt generated is removed.

[57] The composition of an element at time step n is defined as

$$C_{i,l}^n = \frac{m_{i,l}^n}{M_l^n} \qquad C_{i,s}^n = \frac{m_{i,s}^n}{M_s^n}. \tag{B8}$$

We also define the change in melt fraction between time steps as

$$\delta\mathcal{F} = \frac{M_l^{n+1}}{M_s^n}. \tag{B9}$$

From equation (B6), if we divide through by M_s^n then we find

$$1 - \delta\mathcal{F} = \frac{M_s^{n+1}}{M_s^n}. \tag{B10}$$

Likewise, from dividing equation (B7) by M_s^n, and substituting from the definitions of the composition of elements in solid and melt (equation (B8)) and the change in melt fraction (equation (B9)) then we find

$$C_{i,s}^n = C_{i,s}^{n+1}(1 - \delta\mathcal{F}) + C_{i,l}^{n+1}\delta\mathcal{F}, \tag{B11}$$

and for the melt composition, from equation (B3),

$$C_{i,l}^{n+1} = \frac{C_{i,s}^n}{D_i}. \tag{B12}$$

Once melt and solid have been separated, the solid composition is the advected following equation (A3), using the Petrov-Galerkin method [*Brooks and Hughes*, 1982].

B2. Rare Earth Melt Composition Parameterization

[58] The bulk distribution coefficients, D_i, for each element take the form of constant Berthold-Nernst partition coefficients for the different mineral facies. The peridotite facies composition, either plagioclase, spinel or garnet, of the mantle within the melting region is taken to be simply dependent on pressure and temperature [*McKenzie and O'Nions*, 1991]. The decompressing mantle will melt as it passes through the stability fields of garnet, spinel and plagioclase peridotites. Note, amphibole peridotite is not modeled as wet melting in the mid-ocean ridge and rifting scenario is too deep and at too high a temperature for amphibole to be stable [*Grove et al.*, 2006; *Médard et al.*, 2006]. Following [*McKenzie and O'Nions*, 1991], the plagioclase stability field is defined as at depths shallower than 25 km for all temperatures; the spinel stability field is defined as between 35 km depth and the spinel-out boundary,

$$p_{spinel-out} = \frac{T + 400}{666.7}, \tag{B13}$$

and finally the garnet stability field, which is at depths greater than the garnet-in boundary,

$$p_{garnet-in} = \frac{T + 533}{666.7}, \tag{B14}$$

where p is pressure in Pa and T in °C is the temperature in the mantle. The Berthold-Nernst partition coefficient is then given as the sum of the constituent mineral partition coefficients, $\mathcal{D}_{mineral}$, depending on the proportion of minerals within the facies stability field, $P_{mineral}$, (Tables 2 and B1),

$$D_{i,facies} = \sum_k P_{i,k}\mathcal{D}_{i,k}, \tag{B15}$$

where i is the element and k is the mineral. If the temperature and depth fall between these stability fields then the Berthold-Nernst partition coefficient is calculated by linear interpolation between the values within the stability fields.

Appendix C: Decompression Melting of a Depleted Mantle Source

[59] We compare our incremental batch melting model with the simple fractional and batch melting curves for the three peridotite facies through which melting occurs. The REE composition from simple

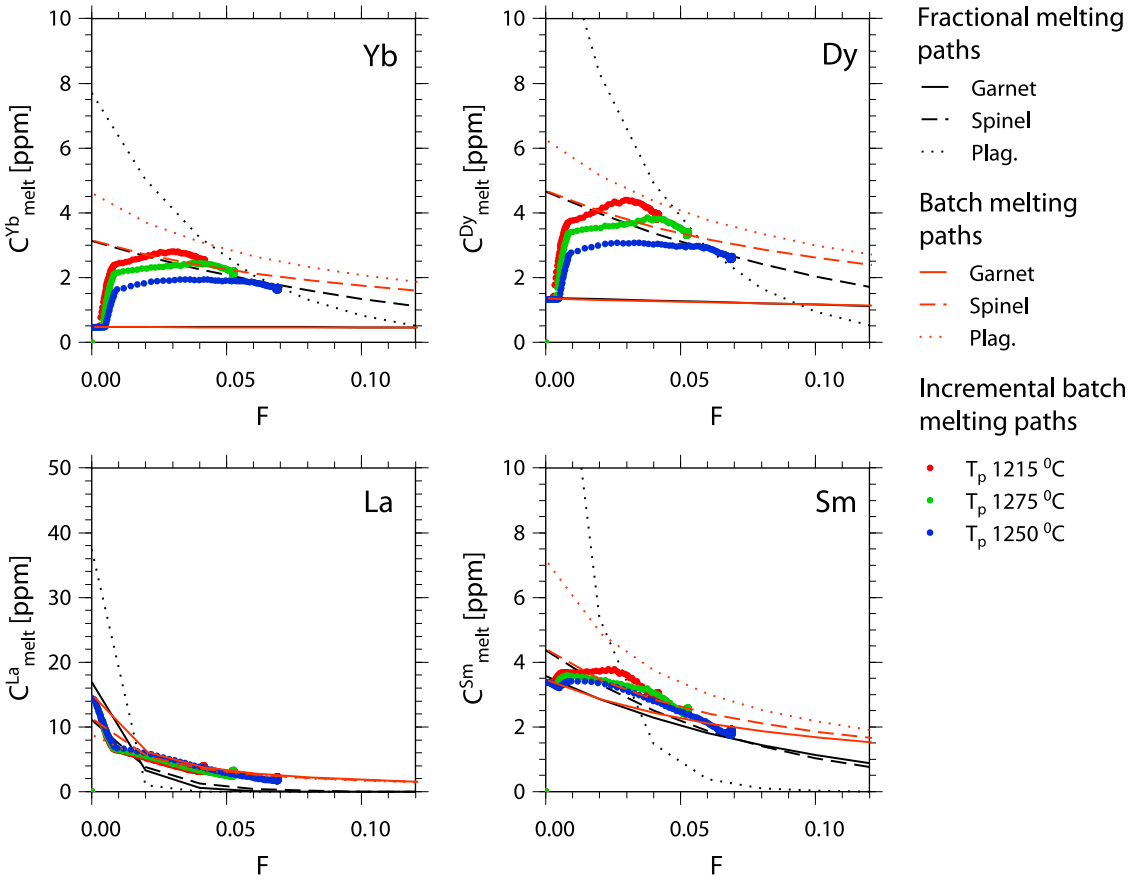

Figure C1. A comparison of the fractional (black solid, dashed, and dotted lines) and batch (red solid, dashed, and dotted lines) melting curves for the plagioclase, spinel, and garnet peridotite stability fields with our incremental batch melting model of the formation of Seychelles-Laxmi Ridge margins. Mantle background temperature is either 1250, 1275, or 1315°C, and half-spreading rates are 60 mm yr^{-1}. The REE compositions for the incremental batch melting are plotted against the mean melt fraction and evolve through time where at time zero the melt fraction is zero.

fractional melting is predicted using [from *Langmuir et al.*, 1992]

$$\frac{C_{i,l}}{C_0} = \frac{1}{D_i}(1-F)^{\left(\frac{1-D}{D}\right)}, \tag{C1}$$

and for simple batch melting,

$$\frac{C_{i,l}}{C_0} = \frac{1}{F(1-D)+D}, \tag{C2}$$

where F is melt depletion, D is the bulk distribution coefficient and C_0 is the initial source mantle composition. The incremental batch melting model as would be expected is between these two end member cases (Figure C1).

[60] Melt production within the geodynamic models is initially deep and is in the stability field of garnet peridotite. This pattern is reproduced within the REE compositions, which for the heavy REE (HREE; for example Dy and Yb), are initially close to the simple batch or fractional melting curve for garnet (Figure C1). As melting progresses and the model evolves, melting is shallower and mainly in the spinel peridotite stability fields. This is as expected for normal mid-ocean ridge dynamics [*McKenzie and O'Nions*, 1991]. For the lighter rare earth elements (LREE; for example La), incremental batch melting predicts melt compositions that are greater than the simple fractional melting curves would predict and more like simple batch melting (Figure C1).

Acknowledgments

[61] We would like to thank Simon Dean and John Hopper for their early input to this work. This work was funded by the UK Natural Environment Research Council grants NER/A/S/2000/01332, NER/A/S/2000/01390, and NER/A/S/2000/01391, and it was also partially supported by the NERC Oceans Margins LINK thematic program through a studentship for John Armitage (grant reference R1/2002/11).

References

Albarede, F. (1995), *Introduction to Geochemical Modelling*, Cambridge Univ. Press, Cambridge, U. K.

Anderson, D. L. (1994), The sublithospheric mantle as the source of continental flood basalts: the case against the continental lithosphere and plume head reservoirs, *Earth Planet. Sci. Lett.*, *123*, 269–280.

Anderson, D. L. (2000), The thermal state of the upper mantle: No role for mantle plumes, *Geophys. Res. Lett.*, *27*, 3623–3626.

Armitage, J. J., T. J. Henstock, T. A. Minshull, and J. R. Hopper (2008), Modelling the composition of melts formed during continental break-up of the North Atlantic, *Earth Planet. Sci. Lett.*, *269*, 248–258, doi: 10.1016/j.epsl.2008.02.024.

Armitage, J. J., T. J. Henstock, T. A. Minshull, and J. R. Hopper (2009), Lithospheric controls on the rifting of continents at slow rates of extension: Application to the North Atlantic, *Geochem. Geophys. Geosyst.*, *10*, Q06018, doi: 10.1029/2009GC002404.

Armitage, J. J., J. S. Collier, and T. A. Minshull (2010), The importance of rift history for volcanic margin formation, *Nature*, *465*, 913–917, doi: 10.1038/nature09063.

Artemieva, I. M., and W. D. Mooney (2001), Thermal thickness and evolution of Precambrian lithosphere: A global study, *J. Geophys. Res.*, *106*, 16,387–16,414.

Asimow, P. D., and C. H. Langmuir (2003), The importance of water to oceanic mantle melting regimes, *Nature*, *421*, 815–820.

Behn, M. D., and P. B. Kelemen (2003), Relationship between seismic P-wave velocity and the composition of anhydrous igneous and meta-igneous rocks, *Geochem. Geophys. Geosyst.*, *4*(5), 1041, doi:10.1029/2002GC000393.

Bernard, A., and M. Munschy (2000), Were the Mascarene and Laxmi Basins (western Indian Ocean) formed at the same spreading centre?, *C. R. Acad. Sci., Ser. IIa*, *330*(11), 777–783.

Bhattacharji, S., N. Chatterjee, J. M. Wampler, P. N. Nayak, and S. S. Deshmukh (1996), Indian intraplate and continental margin rifting, lithospheric extension, and mantle upwelling in Deccan flood basalt volcanism near the K/T boundary: Evidence from mafic dike swarms, *J. Geol.*, *104*, 379–398.

Bhattacharya, G. C., A. K. Chaubey, G. P. S. Murty, K. V. L. N. S. Sarma, V. Subrahmanyam, and K. S. Krishna (1994), Evidence for seafloor spreading in the Laxmi Basin, northeastern Arabian Sea, *Earth Planet. Sci. Lett.*, *125*, 211–220.

Bown, J. W., and R. S. White (1994), Variation with spreading rate of oceanic crust thickness and geochemistry, *Earth Planet. Sci. Lett.*, *121*, 435–449.

Braun, M. G., G. Hirth, and E. M. Parmentier (2000), The effects of deep damp melting on mantle flow and melt generation beneath mid-ocean ridges, *Earth Planet. Sci. Lett.*, *176*, 339–356.

Brooks, A. N., and T. J. R. Hughes (1982), Streamline upwind/Petrov-Galerkin formulations for convection dominated flows with particular emphasis on the incompressible Navier-Stokes equations, *Comput. Methods Appl. Mech. Eng.*, *32*, 199–259.

Burov, E., and L. Guillou-Frottier (2005), The plume head-continental lithosphere interaction using a tectonically realistic formulation for the lithosphere, *Geophys. J. Int.*, *161*, 469–490.

Cambell, I. H. (2007), Testing the plume theory, *Chem. Geol.*, *241*, 152–176.

Collier, J. S., V. Sansom, O. Ishizuka, R. N. Taylor, T. A. Minshull, and R. B. Whitmarsh (2008), Age of Seychelles-India break-up, *Earth Planet. Sci. Lett.*, *272*, 264–277, doi:10.1016/j.epsl.2008.04.045.

Collier, J. S., T. A. Minshull, J. O. S. Hammond, R. B. Whitmarsh, J. M. Kendal, V. Sansom, C. I. Lane, and G. Rumpker (2009), Factors controlling the degree of magmatism during continental breakup: New insights from a wide-angle seismic experiment across the conjugate Seychelles-Indian margins, *J. Geophys. Res.*, *114*, B03101, doi:10.1029/2008JB005898.

Connelly, J. A. D. (1990), Multivariable phase diagrams: an algorithm based on generalised thermodynamics, *Am. J. Sci.*, *290*, 666–718.

Cordery, M. J., and J. Phipps Morgan (1993), Convection and melting at mid-ocean ridges, *J. Geophys. Res.*, *98*, 19,477–19,504.

Corti, G., J. van Wijk, M. Bonini, D. Sokoutis, S. Cloetingh, F. Innocenti, and P. Manetti (2003), Transition from continental break-up to punctiform seafloor spreading: How fast, asymmetric and magnetic, *Geophys. Res. Lett.*, *30*(12), 1604, doi: 10.1029/2003GL017374.

Courtillot, V. E., and P. R. Renne (2003), On the ages of flood basalt events, *C. R. Geosci.*, *335*, 113–140.

Courtillot, V., C. Jaupart, I. Manighetti, P. Tapponnier, and J. Besse (1999), On causal links between flood basalts and continental breakup, *Earth Planet. Sci. Lett.*, *166*, 177–195.

Dean, S. M., B. J. Murton, T. A. Minshull, T. A. Henstock, and R. S. White (2008), An integrated kinematic and geochemical model to determine lithospheric extension and mantle temperatures from syn-rift volcanic compositions, *Earth Planet. Sci. Lett.*, *278*, 26–39, doi:10.1016/j.epsl.2008.11.012.

Dickin, A. P., A. E. Fallick, A. N. Halliday, R. M. Macintyre, and W. E. Stephens (1986), An isotopic and geochronological investigation of the younger igneous rocks of the Seychelles microcontinent, *Earth Planet. Sci. Lett.*, *81*, 46–56.

Dixit, M., H. C. Tewari, and C. V. Rao (2010), Two-dimensional velocity model of the crust beneath the South Cambay Basin, India from refraction and wide-angle reflection data, *Geophys. J. Int.*, *181*, 635–652, doi: 10.1111/j.1365-246X.2010.04539x.

Dixon, J. E., L. Leist, C. Langmuir, and J. Schilling (2002), Recycled dehydrated lithosphere observed in plume-influenced mid-ocean-ridge basalt, *Nature*, *420*, 385–388.

Ebinger, C. J., and N. H. Sleep (1998), Cenozoic magmatism throughout east Africa resulting from impact of a single plume, *Nature*, *395*, 788–791.

Frey, F. A. (1969), Rare earth abundances in high-temperature peridotite intrusion, *Geochim. Cosmochim. Acta*, *33*, 1429–1447, doi:10.1016/0016-7037(69)90183-5.

Gaina, C., R. D. Müller, B. Brown, and T. Ishihara (2007), Break-up and early seafloor spreading between India and Antarctica, *Geophys. J. Int.*, *170*, 151–169.

Gradstein, F. M., J. G. Ogg, and A. G. Smith (2005), *A Geologic Timescale 2004*, Cambridge Univ. Press, Cambridge, U. K.

Grove, T. L., N. Chatterjee, S. W. Parman, and E. Médard (2006), The influence of H_2O on mantle wedge melting, *Earth Planet. Sci. Lett.*, *249*, 74–89, doi: 10.1016/j.epsl.2006.06.043.

Gunnell, Y., K. Gallagher, A. Carter, M. Widdowson, and A. J. Hurford (2003), Denudation history of the continental margin of western peninsular India since the early Mesozoic-reconciling apatite fission-track data with geomorphology, *Earth Planet. Sci. Lett.*, *215*, 187–201.

Halkett, A., N. White, K. Chandra, and N. K. Lal (2001), Dynamic uplift of the Indian peninsula and the reunion

plume, *Eos Trans. AGU*, *82*(47), Fall Meet. Suppl., Abstract T11A-0845.

Herzberg, C., P. D. Asimow, N. Arndt, Y. Niu, C. M. Lesher, J. G. Fitton, M. J. Cheedle, and A. D. Saunders (2007), Temperatures in ambient mantle and plumes: Constraints from basalts, picrites, and komatiites, *Geochem. Geophys. Geosyst.*, *8*, Q02006, doi:10.1029/2006GC001390.

Hill, R. I., I. H. Campbell, G. F. Davies, and R. W. Griffiths (1992), Mantle plumes and continental tectonics, *Science*, *256*, 186–193.

Hirschmann, M. M. (2006), Water, melting, and the deep Earth H_2O cycle, *Annu. Rev. Earth Planet. Sci.*, *34*, 629–653, doi:10.1146/annurev-.earth.34.031405.125211.

Hirschmann, M. M., P. D. Asimow, M. S. Ghiorso, and E. M. Stopler (1999), Calculation of peridotite partial melting from thermodynamic models of minerals and melts. III. Controls on isobaric melt production and the effect of water on melt production, *J. Petrol.*, *40*, 831–851.

Hirth, G., and D. L. Kohlstedt (1996), Water in the oceanic upper mantle: Implications for rheology, melt extraction and the evolution of the lithosphere, *Earth Planet. Sci. Lett.*, *144*, 93–108.

Holland, T. J. B., and R. Powell (1998), An internally consistent thermodynamic data set of phases of petrological interest, *J. Metamorph. Geol.*, *16*, 309–343.

Holtzman, B. K., D. L. Kohlstedt, M. E. Zimmerman, F. Heidelbach, T. Hiraga, and J. Hustoft (2003), Melt segregation and strain partitioning: implications for seismic anisotropy and mantle flow, *Science*, *301*, 1227–1230.

Hooper, P. R. (1990), The timing of crustal extension and the eruption of continental flood basalts, *Nature*, *345*, 246–249.

Hooper, P., M. Widdowson, and K. Simon (2010), Tectonic setting and timing of the final Deccan flood basalt eruptions, *Geology*, *38*, 839–843.

Ito, G., J. Lin, and C. W. Gable (1996), Dynamics of mantle flow and melting at ridge-centred hotspot: Iceland and the Mid-Atlantic Ridge, *Earth Planet Sci. Lett*, *144*, 53–74.

Ito, G., Y. Shen, G. Hirth, and C. J. Wolfe (1999), Mantle flow, and dehydration of the Iceland mantle plume, *Earth Planet. Sci. Lett.*, *165*, 81–96.

Jurine, D., C. Jaupart, G. Brandeis, and P. J. Tackley (2005), Penetration of mantle plumes through depleted lithosphere, *J. Geophys. Res.*, *110*, B10104, doi: 10.1029/2005JB003751.

Kelemen, P. B., G. Hirth, N. Shimizu, M. Spiegelman, and H. J. B. Dick (1997), A review of melt migration processes in the adiabatically upwelling mantle beneath oceanic spreading ridges, *Philos. Trans. R. Soc. A*, *355*, 283–318.

Kent, R. W., M. Storey, and A. D. Saunders (1992), Large igneous provinces: Sites of plume impact or plume incubation, *Geology*, *20*, 891–894.

Klein, E. M. (2004), Geochemistry of the igenous oceanic crust, in *Treatise on Geochemistry*, vol. 3, *The Crust*, edited by R. L. Rudnick, pp. 433–463, Elsevier, Amsterdam.

Kojitani, H., and M. Akaogi (1997), Melting enthalpies of mantle peridotite: Calorimetic determinations in the system CaO-MgO-Al_2O_3-SiO_2 and application to magma generation, *Earth Planet. Sci. Lett.*, *153*, 209–222.

Korenaga, J., P. B. Kelemen, and W. S. Holbrook (2002), Methods for resolving the origin of large igneous provinces from crustal seismology, *J. Geophys. Res.*, *107*(B9), 2178, doi: 10.1029/2001JB001030.

Kumar, P., X. Yuan, M. R. Kumar, R. Kind, X. Li, and P. K. Chadha (2007), The rapid drift of the Indian tectonic plate, *Nature*, *449*, 894–897, doi: 10.1038/nature06214.

Langmuir, H. H., E. M. Klein, and T. Plank (1992), Petrological systematics of mid-ocean ridge basalts: constraints on melt generation beneath ocean ridges, in *Mantle Flow and Melt Generation at Mid-Ocean Ridges*, *Geophys. Monogr. Ser.*, vol. 71, edited by J. Phipps Morgan, D. K. Blackman, and J. M. Sinton, pp. 183–280, AGU, Washington D. C.

Mahoney, J. J., R. A. Duncan, W. Khan, E. Gnos, and G. R. McCormick (2002), Cretaceous volcanic rocks of the South Tethyan suture zone, Pakistan: Implications for the Reunion hotspot and Deccan Traps, *Earth Planet. Sci. Lett.*, *203*, 295–310.

Malod, J. A., L. Droz, B. M. Kemal, and P. Patriat (1997), Early spreading and continental to oceanic basement transition beneath the Indus deep-sea fan: northeastern Arabian Sea, *Mar. Geol.*, *141*, 221–235.

McKenzie, D. P. (1984), The generation and compaction of partially molten rock, *J. Petrol.*, *25*, 713–765.

McKenzie, D. P., and M. J. Bickle (1988), The volume and composition of melt generated by extension of the lithosphere, *J. Petrol.*, *29*, 625–679.

McKenzie, D., and R. K. O'Nions (1991), Partial melt distribution from inversion of rare earth element concentrations, *J. Petrol.*, *32*, 1021–1091.

McKenzie, D., J. Jackson, and K. Priestley (2005), Thermal structure of oceanic and continental lithosphere, *Earth Planet. Sci. Lett.*, *233*, 337–349.

Médard, E., M. W. Schmidt, P. Schiano, and L. Ottolini (2006), Melting of amphibole-bearing wehrlites and experimental study on the origin of ultra-calcic nepheline-normative melts, *J. Petrol.*, *47*, 481–504, doi: 10.1093/petrology/egi083.

Mei, S., and D. L. Kohlstedt (2000), Influence of water on plastic deformation of olivine aggregates 2. Dislocation creep, *J. Geophys. Res.*, *105*, 21,471–21,481.

Minshull, T. A., C. I. Lane, J. S. Collier, and R. B. Whitmarsh (2008), The relationship between rifting and magmatism in the northeastern Arabian Sea, *Nat. Geosci.*, *1*, 463–467.

Mittelsteadt, E., G. Ito, and M. D. Behn (2008), Mid-ocean ridge jumps associated with hotspot magmatism, *Earth Planet. Sci. Lett.*, *266*, 256–270, doi: 10.1016/j.epsl.2007.10.055.

Mittelsteadt, E., G. Ito, and J. van Hunen (2011), Repeat ridge jumps associated with plume/ridge interaction, melt transport, and ridge migration, *J. Geophys. Res.*, *116*, B01102, doi:10.1029/2010JB007504.

Moresi, L., and V. S. Solomatov (1995), Numerical investigation of 2D convection with extremely large viscosity variations, *Phys. Fluids*, *7*, 2154–2162.

Naini, B. R., and M. Talwani (1982), Structural framework and the evolutionary history of the continental margin of western India, in *Studies in Continental Margin Geology*, edited by J. S. Watkins and C. L. Drake, *AAPG Mem.*, *34*, 167–191.

Nielsen, T. K., and J. R. Hopper (2004), From rift to drift: Mantle melting during continental breakup, *Geochem. Geophys. Geosyst.*, *5*, Q07003, doi:10.1029/2003GC000662.

Pande, K. (2002), Age and duration of the Deccan Traps, India: A review of radiometric and paleomagnetic constraints, *Proc. Indian Acad. Sci*, *111*, 115–123.

Phipps Morgan, J. (2001), Thermodynamics of pressure release melting of a veined plum pudding mantle, *Geochem. Geophys. Geosyst.*, *2*, 1001, doi: 10.1029/2000GC000049.

Plank, T., M. Spiegelman, C. H. Langmuir, and D. W. Forsyth (1995), The meaning of 'mean F': Clarifying the mean extent of melting at ocean ridges, *J. Geophys. Res.*, *100*, 15,045–15,052.

Plummer, P. S. (1995), Ages and geological significance of the igneous rocks from Seychelles, *J. Afr. Earth Sci.*, *20*, 91–101.

Priestly, K., and D. McKenzie (2006), The thermal structure of the lithosphere from shear velocities, *Earth Planet. Sci. Lett.*, *244*, 285–301, doi: 10.1016/j.epsl.2006.01.008.

Rehkamper, M., and A. W. Hofmann (1997), Recycled ocean crust and sediment in Indian Ocean MORB, *Earth Planet. Sci. Lett.*, *147*, 93–106.

Ribe, N. M., and U. R. Christensen (1994), Three-dimensional modeling of plume-lithosphere interaction, *J. Geophys. Res.*, *99*, 669–682.

Richards, M. A., R. A. Duncan, and V. E. Courtillot (1989), Flood basalts and hot spot tracks: Plume heads and tails, *Science*, *246*, 103–107.

Royer, J. Y., A. K. Chaubey, J. Dyment, G. C. Bhattacharya, K. Shrivas, V. Yatheesh, and T. Ramprasad (2002), Paleogene plate tectonic evolution of the Arabian Sea and Eastern Somali Basin, in *The Tectonic and Climatic Evolution of the Arabian Sea Region*, edited by P. D. Clift et al., *Geol. Soc. Spec. Publ.*, *195*, 7–23.

Saunders, A. D., S. M. Jones, L. A. Morgan, K. L. Pierce, M. Widdowson, and Y. G. Xu (2007), Regional uplift associated with continental large igneous provinces: The roles of mantle plumes and the lithosphere, *Chem. Geol.*, *241*, 282–318.

Scott, D. R. (1992), Small-scale convection and mantle melting beneath mid-ocean ridges, in *Mantle Flow and Melt Generation at Mid-Ocean Ridges*, *Geophys. Monogr. Ser.*, vol. 71, edited by J. Phipps Morgan, D. K. Blackman, and J. M. Sinton, pp. 327–352, AGU, Washington D. C.

Sheth, H. C. (2000), The timing of crustal extension, diking, and eruption of the Deccan flood basalts, *Int. Geol. Rev.*, *42*, 1007–1016.

Sleep, N. H. (1996), Lateral flow of hot plume material ponded at sublithospheric depths, *J. Geophys. Res.*, *101*, 28,065–28,083.

Sleep, N. H. (2007), Edge-modulated stagnant-lid convection and volcanic passive margins, *Geochem. Geophys. Geosyst.*, *8*, Q12004, doi:10.1029/2007GC001672.

Sobolev, S. V., and A. Y. Babeyko (1994), Modelling of mineralogical composition, density and elastic wave velocities in anhydrous magmatic rocks, *Surv. Geophys.*, *15*, 515–544.

Spiegelman, M. (1996), Geochemical consequences of melt transport in 2-D: The sensitivity of trace elements to mantle dynamics, *Earth Planet. Sci. Lett.*, *139*, 115–132.

Stracke, A., B. Bourdon, and D. McKenzie (2006), Melt extraction in the Earth's mantle: constraints from U-Th-Pa-Ra studies in oceanic basalts, *Earth Planet. Sci. Lett.*, *244*, 97–112, doi:10.1016/j.epsl.2006.01.057.

Sun, S. S., and W. F. McDonough (1989), Chemical and isotopic systematics of oceanic basalts: implications for mantle composition and processes, in *Magmatism in the Ocean Basins*, edited by A. D. Saunders and M. J. Norry, *Geol. Soc. Spec. Publ.*, *42*, 313–345.

Thompson, R. N., and S. A. Gibson (1991), Subcontinental mantle plumes, hotspots and preexisting thinspots, *J. Geol. Soc.*, *148*, 973–977.

Torres-Alvarado, I. S., S. P. Verma, H. Palacios-Berruete, M. Guevara, and O. Y. Gonzalez-Castillo (2003), DC_BASE: a database system to manage Nernst distribution coefficients and its application to partial melting modeling, *Comput. Geosci.*, *29*, 1191–1198, doi:10.1016/S0098-3004(03)00132-8.

Wasylenki, L. E., M. B. Baker, A. J. R. Kent, and E. M. Stopler (2003), Near-solidus melting of the shallow upper mantle: Partial melting experiments on depleted peridotite, *J. Petrol.*, *44*, 116–1191.

White, R. S., and D. McKenzie (1995), Mantle plumes and flood basalts, *J. Geophys. Res.*, *100*, 17,543–17,585.

White, R. S., and D. P. McKenzie (1989), Magmatism at rift zones: the generation of volcanic continental margins and flood basalts, *J. Geophys. Res.*, *94*, 7685–7729.

Yamasaki, T., and L. Gernigon (2009), Styles of lithospheric extension controlled by underplated mafic bodies, *Tectonophysics*, *468*, 169–184.

Yamasaki, T., and L. Gernigon (2010), Redistribution of the lithosphere deformation by the emplacement of underplated mafic bodies: Implications for microcontinent formation, *J. Geol. Soc.*, *167*, 961–971.

Yatheesh, V., G. C. Bhattacharya, and J. Dyment (2009), Early oceanic opening off Western India-Pakistan margin: The Gop Basin revisited, *Earth Planet. Sci. Lett.*, *284*, 399–408, doi: 10.1016/j.epsl.2009.04.044.